Received: 16 December 2020 | Revised: 28 February 2021 | Accepted: 15 March 2021

DOI: 10.1111/cmi.13327

RESEARCH ARTICLE

WILEY

HrpB4 from *Xanthomonas campestris pv. vesicatoria* acts similarly to SctK proteins and promotes the docking of the predicted sorting platform to the type III secretion system

Christian Otten | **Daniela Büttner**

Institute of Biology, Department of Genetics, Martin Luther University Halle-Wittenberg, Halle (Saale), Germany

Correspondence
Daniela Büttner, Institute of Biology, Department of Genetics, Martin Luther University Halle-Wittenberg, Weinbergweg 10, 06120 Halle (Saale), Germany.
Email: daniela.buettner@genetik.uni-halle.de

Funding information
Deutsche Forschungsgemeinschaft, Grant/Award Numbers: BU 2145/9-1, BU 2145/10-1

Abstract

The Gram-negative bacterium *Xanthomonas campestris* pv. *vesicatoria* is the causal agent of bacterial spot disease on pepper and tomato plants. Pathogenicity of *X. campestris* pv. *vesicatoria* depends on a type III secretion (T3S) system which translocates bacterial effector proteins into plant cells. At least nine membrane-associated and cytoplasmic components of the secretion apparatus are homologous to corresponding Sct (secretion and cellular translocation) proteins from animal pathogens, suggesting a similar structural organisation of T3S systems in different bacterial species. T3S in *X. campestris* pv. *vesicatoria* also depends on non-conserved proteins with yet unknown function including the essential pathogenicity factor HrpB4. Here, we show that HrpB4 localises to the cytoplasm and the bacterial membranes and interacts with the cytoplasmic domain of the inner membrane (IM) ring component HrcD and the cytoplasmic HrcQ protein. The analysis of HrpB4 deletion derivatives revealed that deletion of the N- or C-terminal protein region affects the interaction of HrpB4 with HrcQ and HrcD as well as its contribution to pathogenicity. HrcQ is a component of the predicted sorting platform, which was identified in animal pathogens as a dynamic heterooligomeric protein complex and associates with the IM ring via SctK proteins. HrcQ complex formation was previously shown by fluorescent microscopy analysis and depends on the presence of the T3S system. In the present study, we provide experimental evidence that the absence of HrpB4 severely affects the docking of HrcQ complexes to the T3S system but does not significantly interfere with HrcQ complex formation in the bacterial cytoplasm. Taken together, our data suggest that HrpB4 links the predicted cytoplasmic sorting platform to the IM rings of the T3S system.

KEYWORDS
ATPase complex, C ring, inner membrane ring, plant-pathogenic bacterium, SctK protein family, sorting platform, type III secretion

1 | INDRODUCTION

The Gram-negative plant-pathogenic bacterium *Xanthomonas campestris* pv. *vesicatoria* (also designated *Xanthomonas euvesicatoria*) is the causal agent of bacterial spot disease in pepper and tomato plants and one of the model organisms for the molecular analysis of plant–pathogen interactions (Büttner & Bonas, 2010; Jones, Lacy, Bouzar, Stall, & Schaad, 2004; Timilsina et al., 2020). In natural infections, *X. campestris* pv. *vesicatoria* enters the plant tissue via openings on the leaf surface such as stomata or wounds, and multiplies locally in the plant intercellular spaces. Bacterial pathogenicity depends on effector proteins which interfere with host cellular processes such as defence responses to the bacterial benefit (Büttner, 2016). Bacterial effectors are often translocated into plant cells by the type III secretion (T3S) system which is an essential pathogenicity factor of most Gram-negative plant- and animal-pathogenic bacteria. T3S systems consist of more than 20 proteins which are often encoded by a single gene cluster (Büttner, 2012; Ghosh, 2004). According to sequence conservations and similarities in the genetic organisation and regulation, T3S systems from plant-pathogenic bacteria have been grouped into Hrp1 (hypersensitive response and pathogenicity 1)-T3S systems (in *Erwinia* spp. and *Pseudomonas syringae* pathovars) and Hrp2-T3S systems (in *Xanthomonas* spp. and *Ralstonia solanacearum*) (Alfano & Collmer, 1997; Bogdanove et al., 1996; Troisfontaines & Cornelis, 2005). The Hrp designation refers to the contribution of T3S systems to bacterial pathogenicity in susceptible plants and to the induction of effector-triggered defence responses in resistant plants (Bogdanove et al., 1996; Tampakaki et al., 2010). Recognition of type III effectors in resistant plants depends on the presence of corresponding plant resistance genes and often leads to the induction of a hypersensitive response (HR), a rapid local cell death at the infection site (Gill, Lee, & Mysore, 2015; Jones & Dangl, 2006).

The *hrp* gene cluster from *X. campestris* pv. *vesicatoria* contains 25 genes, organised in eight operons, and encodes structural and helper proteins of the T3S system (Büttner & Bonas, 2002). The two transcriptional regulators HrpG and HrpX, which activate *hrp* gene expression *in planta* or in specific minimal media, are encoded outside the *hrp* gene cluster (Büttner & Bonas, 2010; Wengelnik & Bonas, 1996; Wengelnik, Van den Ackerveken, & Bonas, 1996). Comparative sequence analyses revealed that 11 *hrp* gene products–designated *hrc* for *hrp* conserved–are conserved in plant- and/or animal-pathogenic bacteria and presumably constitute the core components of the T3S system. The corresponding proteins from animal pathogens were designated Sct (secretion and cellular translocation), followed by a letter which refers to the nomenclature of T3S system components from *Yersinia* spp. (Bogdanove et al., 1996). The sequence similarities between Sct and Hrc proteins suggest that T3S systems from animal and plant pathogens share a similar architecture.

In animal-pathogenic bacteria, structural studies revealed that the membrane-spanning part of T3S systems consists of ring structures in the outer membrane (OM) and inner membrane (IM) which are linked by a central periplasmic rod (Deng et al., 2017; Lara-Tejero & Galan, 2019; Wagner et al., 2018). The OM ring is assembled by members of the SctC secretin family and is associated with an extracellular pilus-like appendage (Büttner, 2012). The IM rings consist of oligomeric SctD and SctJ ring complexes, with SctD rings being located on the outer and SctJ rings on the inner side (Lara-Tejero & Galan, 2019). The IM rings surround the export apparatus, which is assembled by SctU, SctV, SctR, SctS and SctT proteins and is associated with the cytoplasmic ATPase SctN which presumably provides the energy for secretion and protein unfolding (Büttner, 2012; Singh & Wagner, 2019; Wagner et al., 2018). The ATPase is located in the centre of the cytoplasmic sorting platform and is linked via SctL to SctQ which forms six pod-like structures at the periphery of the sorting platform (Hu et al., 2015; Lara-Tejero, 2019; Lara-Tejero & Galan, 2019). SctQ proteins are also referred to as C (cytoplasmic) ring components because the homologues FliM and FliN from the flagellar T3S system form a closed ring structure which has, however, not been visualised in translocation-associated T3S systems from animal-pathogenic bacteria (Hu et al., 2015; Kawamoto et al., 2013).

The sorting platform of T3S systems from animal-pathogenic bacteria is a dynamic protein complex, which undergoes assembly and disassembly and switches its localization between the cytoplasm and the T3S system (Diepold et al., 2017; Diepold, Kudryashev, Delalez, Berry, & Armitage, 2015; Notti, Bhattacharya, Lilic, & Stebbins, 2015; Zhang, Lara-Tejero, Bewersdorf, & Galan, 2017). In T3S systems from plant-pathogenic bacteria, which have less intensively been studied than those from animal pathogens, the sorting platform of T3S systems has not yet been identified. We previously reported that the predicted C ring component HrcQ from *X. campestris* pv. *vesicatoria*, which is homologous to SctQ proteins from animal-pathogenic bacteria, forms oligomeric complexes and associates with components of the T3S system (Lorenz, Hausner, & Büttner, 2012). HrcQ interacts with the ATPase complex and the cytoplasmic domains of HrcU and HrcV, which are components of the export apparatus in the IM (Lorenz et al., 2012). Fractionation experiments revealed that HrcQ localises to the bacterial cytoplasm and the membranes under T3S-permissive conditions (Lorenz et al., 2012). The association of HrcQ with the T3S system was recently visualised in situ by the analysis of a HrcQ-sfGFP (superfolder green fluorescent protein) fusion protein which forms fluorescent foci in the presence of a functional T3S system (Hausner, Jordan, Otten, Marillonnet, & Büttner, 2019).

Take Away

- Type III secretion in Xanthomonas campestris pv. vesicatoria depends on HrpB4.
- HrpB4 interacts with HrcQ and the inner membrane ring protein HrcD.
- HrpB4 links the predicted sorting platform to the inner membrane ring.
- HrpB4 likely acts similarly to SctK proteins from animal-pathogenic bacteria.

In the present study, we show that the efficient association and complex formation of HrcQ-sfGFP depends on the non-conserved HrpB4 protein, which is an essential pathogenicity factor of *X. campestris* pv. *vesicatoria* and is encoded in the *hrpB* operon of the *hrp* gene cluster (Rossier, Van den Ackerveken, & Bonas, 2000). Fractionation and in vivo interaction studies revealed that HrpB4 peripherally associates with the bacterial membranes and interacts with the predicted C ring component HrcQ and the cytoplasmic domain of the IM ring protein HrcD. The N- and C-terminal regions of HrpB4 contribute to the interactions with HrcD and HrcQ as well as to pathogenicity. Fluorescence microscopy studies showed that HrpB4 is required for the efficient docking of HrcQ-sfGFP to the T3S system, suggesting that HrpB4 acts as a linker between the IM rings and the predicted sorting platform of the T3S system.

2 | EXPERIMENTAL RESULTS

2.1 | HrpB4 is essential for T3S and effector protein translocation

HrpB4 from *X. campestris* pv. *vesicatoria* is a protein of 209 amino acids and is encoded in the *hrp* gene cluster by the fourth gene of the *hrpB* operon which is located between *hrcJ* and *hrcL* (Figure 1a). Comparative sequence analyses revealed that HrpB4 is conserved in *Xanthomonas* spp. (68 to 96% amino acid identity) and shares sequence similarity with the C-terminal region of HrpB4 from *Ralstonia solanacearum* (34% amino acid identity restricted to amino acids 74–209 of HrpB4) (Figure S1). Deletion of codons 20 to 129 of *hrpB4* from the genome of *X. campestris* pv. *vesicatoria* leads to a loss of pathogenicity and in vitro T3S, suggesting that HrpB4 is an essential pathogenicity factor (Rossier et al., 2000). To confirm that the *hrpB4* mutant phenotype was caused by the absence of HrpB4 and not by a polar effect of the deletion in *hrpB4* on flanking genes, we performed complementation studies. For this, *hrpB4* was ectopically expressed in fusion with a triple C-terminal c-Myc epitope-encoding sequence under control of the *lac* promoter in *X. campestris* pv. *vesicatoria* strain 85–10Δ*hrpB4* in the presence and absence of HrpG*, which is a constitutively active version of the key regulator HrpG. HrpG* allows *hrp* gene expression under non-inducing conditions and also leads to enhanced plant reactions (Wengelnik, Rossier, & Bonas, 1999). When bacteria were infiltrated into leaves of pepper plants, the wild-type strain induced water-soaked lesions in susceptible ECW and the HR in resistant ECW-10R pepper plants as expected (Figures 1b and S2). ECW-10R plants elicit the HR upon recognition of the effector protein AvrBs1, which is delivered by *X. campestris* pv. *vesicatoria* strain 85–10 (Minsavage et al., 1990). No plant reactions were visible after infection with *hrpB4* deletion mutants containing the *hrpG* wild-type or the *hrpG** gene, suggesting that constitutive *hrp* gene expression in the presence of HrpG* did not restore pathogenicity in *hrpB4* mutants (Figures 1b and S2). The mutant phenotype was complemented by ectopic expression of *hrpB4-c-myc* with respect to disease symptoms and the HR, suggesting that the loss of pathogenicity was specifically caused by the absence of HrpB4 (Figures 1b and S2).

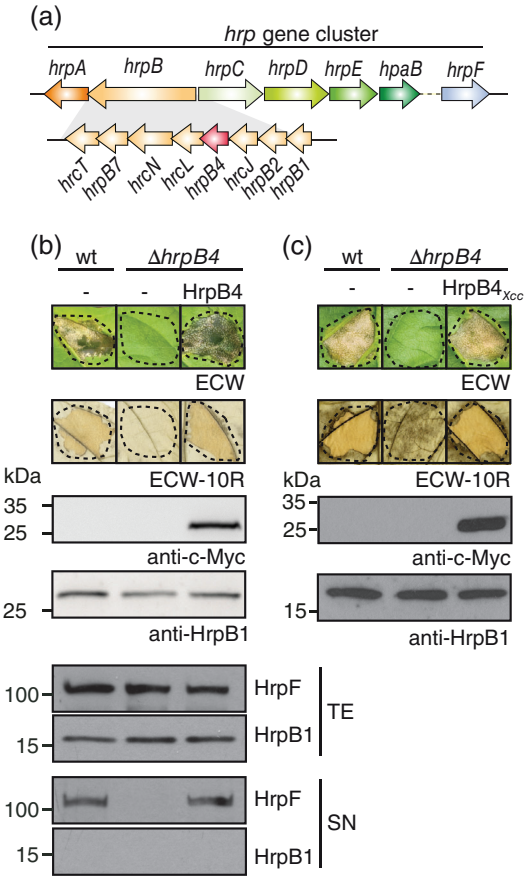

FIGURE 1 Complementation studies with HrpB4 derivatives. (a) Schematic representation of the *hrp* operons and the genes in the *hrpB* operon from *X. campestris* pv. *vesicatoria*. Operons and genes are represented by arrows. (b) Complementation of the *hrpB4* mutant phenotype. *X. campestris* pv. *vesicatoria* strains 85–10 (wt) and 85–10Δ*hrpB4* (Δ*hrpB4*) containing HrpG* and expressing *hrpB4-c-myc* (HrpB4) under control of the *lac* promoter as indicated were infiltrated into leaves of susceptible ECW and resistant ECW-10R pepper plants. Disease symptoms were photographed 8 dpi. For the better visualisation of the HR, leaves of resistant plants were destained in ethanol. Dashed lines indicate the infiltration sites. For protein analysis, bacterial cell extracts were analysed by immunoblotting using a c-Myc epitope-specific antibody. The blot was reprobed with a HrpB1-specific antibody to show equal loading. For the analysis of in vitro T3S, bacteria were incubated in secretion medium, and total cell extracts (TE) and culture supernatants (SN) were analysed by immunoblotting, using antibodies specific for the secreted translocon protein HrpF and the periplasmic HrpB1 protein, respectively. (c) HrpB4 from *X. campestris* pv. *campestris* is functional in *X. campestris* pv. *vesicatoria*. Strains 85–10 (wt) and 85–10Δ*hrpB4* (Δ*hrpB4*) containing HrpG* and an expression construct encoding $HrpB4_{Xcc}$-c-Myc as indicated ($HrpB4_{Xcc}$) were infiltrated into susceptible ECW and resistant ECW-10R pepper plants. Plant reactions were monitored as described in (b). For protein analysis, cell extracts were analysed by immunoblotting using a c-Myc epitope-specific antibody. The blot was reprobed with a HrpB1-specific antibody to show equal loading

For the analysis of T3S in culture, bacteria were cultivated in secretion medium, and cell extracts and culture supernatants were analysed by immunoblotting, using an antibody specific for the secreted translocon protein HrpF. As expected, HrpF was detectable in the culture supernatant of the wild-type strain but not of the *hrpB4* deletion mutant (Figure 1b). HrpF secretion in the *hrpB4* deletion mutant was restored by ectopic expression of *hrpB4-c-myc* (Figure 1b). The blots were reprobed with an antibody against the periplasmic HrpB1 protein to ensure that no cell lysis had occurred (Figure 1b).

To investigate whether the role of HrpB4 is conserved in *Xanthomonas* spp., we also performed complementation studies with HrpB4 from *X. campestris* pv. *campestris* ($HrpB4_{Xcc}$), which shares 68% amino acid identity with HrpB4 from *X. campestris* pv. *vesicatoria* (see above; Figure S1). Ectopic expression of $hrpB4_{Xcc}$-*c-myc* under control of the *lac* promoter in *X. campestris* pv. *vesicatoria hrpB4* deletion mutants restored the wild-type phenotype in susceptible and resistant pepper plants, suggesting that $HrpB4_{Xcc}$ was functional in *X. campestris* pv. *vesicatoria* (Figures 1c and S2). We conclude that the amino acid differences between HrpB4 from *X. campestris* pv. *vesicatoria* and *X. campestris* pv. *campestris* do not significantly interfere with protein function.

2.2 | HrpB4 localises to the bacterial membranes and the cytoplasm

It was previously reported that HrpB4 is not secreted by the T3S system and localises to the bacterial membranes and the cytoplasm (Rossier et al., 2000). To analyse whether HrpB4 associates with the bacterial membranes or is an integral membrane protein, we performed fractionation studies. For this, bacteria were grown in minimal medium at pH 5.3 (T3S-permissive) or pH 7.0 (T3S non-permissive conditions), and soluble and membrane fractions of bacterial lysates were separated by centrifugation. The membrane fractions were subsequently incubated in the presence of 5 M urea to dissociate peripherally attached proteins from the membrane, and integral membrane proteins were separated from membrane-associated proteins by ultracentrifugation. When soluble, membrane-associated and integral membrane protein fractions were analysed by immunoblotting, HrpB4-c-Myc was detected in all fractions irrespective of the growth conditions (Figures 2 and S3). Similar results were obtained when HrpB4-c-Myc was analysed in an *X. campestris* pv. *vesicatoria* strain which lacked the complete *hrp* gene cluster, suggesting that the localization of HrpB4 in the cytoplasm and at the bacterial membranes was independent of the T3S system (Figures 2 and S3). As control, blots were reprobed with antibodies specific for the IM ring protein HrcJ or the cytoplasmic ATPase HrcN. As expected, HrcJ was predominantly present in the membrane and HrcN in the cytoplasmic fractions (Figures 2 and S3). These results suggest that HrpB4 associates with the bacterial membranes which is in agreement with the absence of predicted transmembrane domains in HrpB4.

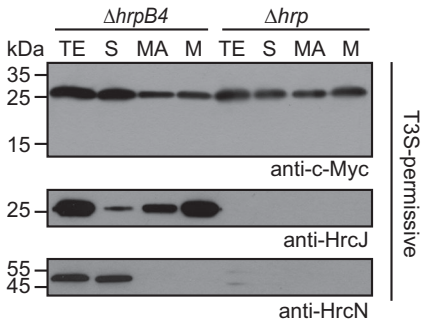

FIGURE 2 Localization studies with HrpB4.*X. campestris* pv. *vesicatoria* strains 85–10Δ*hrp* (Δ*hrp*) and 85–10Δ*hrpB4* (Δ*hrpB4*) both containing HrpG* and expressing *hrpB4-c-myc* under control of the *lac* promoter were incubated under T3S-permissive conditions, and soluble and membrane fractions were separated by ultracentrifugation. Membrane-associated proteins were subsequently separated from integral membrane proteins by ultracentrifugation after treatment of the membrane fractions with 5 M urea. Proteins were analysed by immunoblotting, using antibodies specific for the c-Myc epitope, the IM ring component HrcJ and the cytoplasmic ATPase HrcN. TE, total cell extracts; S, soluble fraction; MA, membrane-associated fractions; M, membrane fraction

2.3 | HrpB4 interacts with the predicted C ring protein HrcQ and the IM ring component HrcD

Given the membrane association of HrpB4, we investigated whether it interacts with cytoplasmic or membrane components of the T3S system. For this, we performed in vivo interaction studies using the bacterial adenylate cyclase-based two hybrid (BACTH) system. The BACTH system is based on the reconstitution of the catalytic domain of the adenylate cyclase (Cya) from two subdomains (T18 and T25) which are analysed as fusions to two potential interaction partners. Protein–protein interaction leads to the assembly of functional Cya and thus to the synthesis of cAMP (Battesti & Bouveret, 2012; Karimova, Pidoux, Ullmann, & Ladant, 1998). In *Escherichia coli* reporter strains lacking the native *cya* gene, cAMP synthesis leads to the activation of the *lac* operon which can be visualised by growing bacterial cultures on indicator plates (Battesti & Bouveret, 2012; Karimova et al., 1998). The original BACTH vectors allowed the classical cloning of genes of interest into a multiple cloning site (mcs) located upstream or downstream of the T18- (vectors pUT18 and pUT18C) or T25-encoding sequences (vectors pKNT25 and pKT25) (Euromedex; Karimova, Ullmann, & Ladant, 2001). The mcs of the original BACTH vectors lacked a reporter gene for selection of positive clones and contained additional coding sequences upstream or downstream of the *T18* and *T25* genes. This results in T25 and T18 fusion proteins with additional N- or C-terminal amino acids depending on the restriction sites chosen for cloning with type II restriction enzymes (Figure S4). We, therefore, generated modified Golden Gate-compatible BACTH vectors which contain *eforRed* as reporter gene for the selection of positive clones and a FLAG

epitope-encoding sequence for immunodetection of the T18 and T25 fusion proteins (Figures 3a and S4) (Liljeruhm et al., 2018).

Using the Golden Gate-compatible BACTH vectors, we analysed possible interactions of HrpB4 with the predicted IM ring components HrcD and HrcJ, the putative C ring protein HrcQ, the cytoplasmic ATPase HrcN and its putative regulator HrcL. Immunoblot analyses showed that all fusion proteins were stably synthesised in *E. coli* (Figure S5). For interaction studies, constructs were transferred into the *E. coli* reporter strain DHM1, and bacterial cultures were spotted on indicator plates. Given that T18 and T25 fusion partners might interfere with protein folding, potential interaction partners were tested as N- and C-terminal fusions to the T18 or T25 domain in all combinations. HrpB4 fusions did not interact with T18 and T25 fusions of HrcJ, HrcN and HrcL but with T18-HrcD and T25-HrcD (Figure 3b). In contrast, no interaction was detectable between HrpB4 fusions and HrcD-T18 or HrcD-T25 (Figure 3b). According to previous topology studies, it is possible that the membrane insertion of HrcD in *E. coli* results in a periplasmic localization of C-terminal T18 or T25 fusion partners, which would likely prevent an interaction with cytoplasmic T25 or T18 fusion proteins (Berger, Robin, Bonas, & Koebnik, 2010). The combination of HrpB4-T25 with T18-HrcQ led to a slight LacZ activity (Figure 3b). We, therefore, repeated the

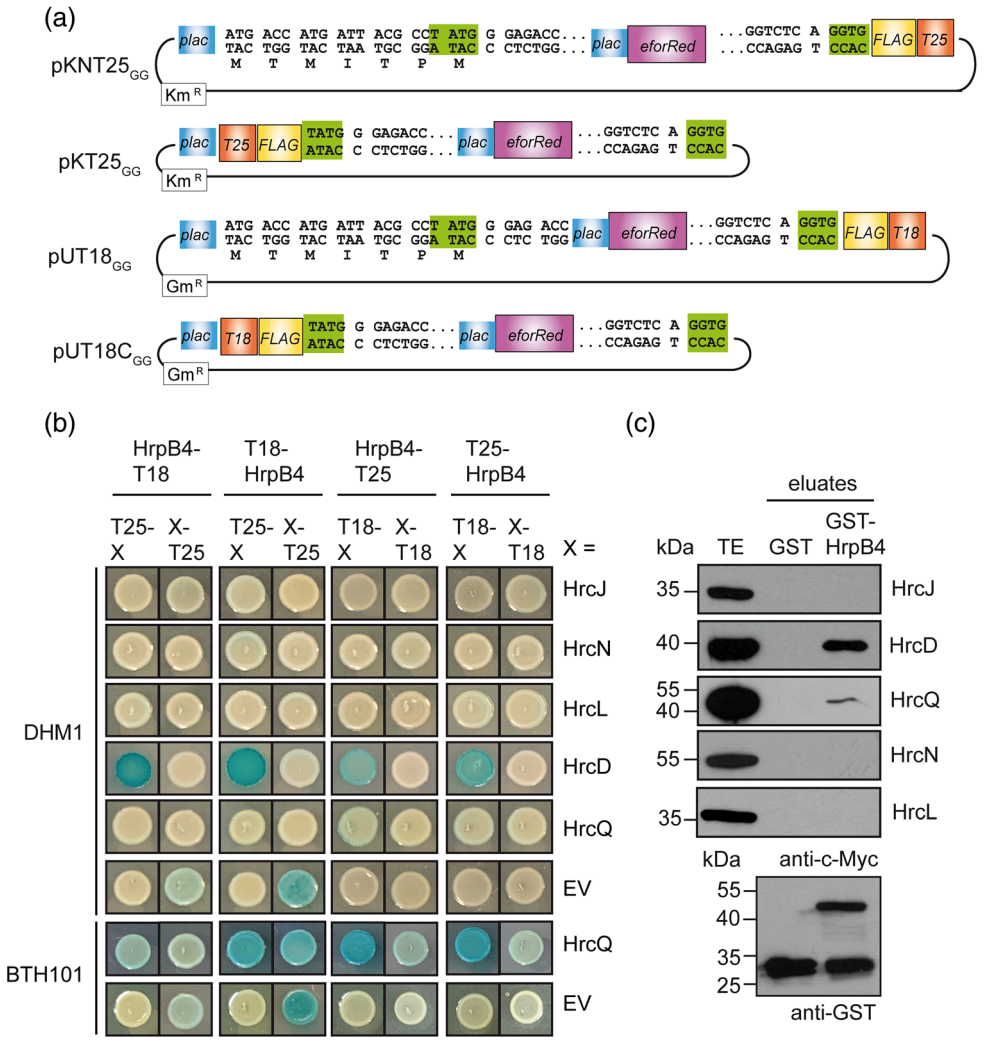

FIGURE 3 HrpB4 interacts with the IM ring component HrcD and the predicted C ring protein HrcQ. (a) Schematic representation of modified Golden Gate-compatible BACTH vectors. BsaI recognition sites flanking the *eforRed* gene expressed under control of the *lac* promoter (*plac*) as well as additional flanking sequences are shown. BsaI fusion sites are highlighted in green. Single letters below the sequences given for vectors pKNT25$_{GG}$ and pUT18$_{GG}$ refer to amino acids resulting from translation initiation at the first AUG start site downstream of the *lac* promoter. Gm, gentamycin; Km, Kanamycin, *plac*, *lac* promoter; R, resistant. (b) Identification of HrpB4 interaction partners by BACTH assays. T25 and T18 fusions were analysed in DHM1 or BTH101 *E. coli* reporter strains as indicated, and bacterial cultures were spotted on indicator plates. Photographs were taken after 3–4 days. EV, empty vector. (c) In vitro interaction of HrpB4 with HrcD and HrcQ. GST and GST-HrpB4 were immobilised on glutathione sepharose and incubated with bacterial lysates containing C-terminally c-Myc epitope-tagged potential HrpB4 interaction partners as indicated. Total cell extracts (TE) and eluted proteins (eluates) were analysed by immunoblotting using c-Myc epitope- and GST-specific antibodies

interaction studies with HrpB4 and HrcQ in the *E. coli* strain BTH101, which grows faster than strain DHM1 and allows a more efficient detection of LacZ activity (Battesti & Bouveret, 2012). Notably, an interaction between HrpB4 and HrcQ fusions was clearly detectable in BTH101 cells which confirms the hypothesis that HrpB4 interacts with the predicted C ring protein HrcQ (Figure 3b).

Unexpectedly, when T18 fusions of HrpB4 were analysed with the empty vector pKNT25 encoding the T25 domain downstream of the multiple cloning site in DHM1 and BTH101 cells, the bacterial cultures were slightly blue. However, no LacZ activity was detectable when T18 fusions of HrpB4 were tested with vector pKT25 encoding T25 upstream of the multiple cloning site or with putative interaction partners expressed from the Golden Gate-compatible vector pKNT25$_{GG}$ (Figure 3b). We, therefore, assume that HrpB4 did not generally interact with the T25 domain but that the fusion of the T25 domain to additional amino acids encoded by the polylinker of vector pKNT25, which is the original vector of the BACTH system, resulted in unspecific binding to HrpB4. Notably, we observed similar false positive interaction signals when combinations of vector pKNT25 with T18 fusions of other T3S system components were tested (data not shown).

To confirm the results of the BACTH assays, we performed in vitro GST pull-down assays. For this, GST and GST-HrpB4 were immobilised on a glutathione sepharose matrix and incubated with bacterial lysates containing C-terminally c-Myc epitope-tagged derivatives of HrcJ, HrcD, HrcQ, HrcN or HrcL. When eluted proteins were analysed by immunoblotting, HrcD-c-Myc and HrcQ-c-Myc coeluted with GST-HrpB4 but not with GST alone (Figure 3c). In contrast, HrcJ-c-Myc, HrcN-c-Myc and HrcL-c-Myc were not detectable in the eluate of GST-HrpB4 (Figure 3c), which is in agreement with the results of the BACTH assays. We conclude from the results of the BACTH assays and the in vitro pull-down experiments that HrpB4 interacts with HrcD and the predicted C ring protein HrcQ. The interaction between HrpB4 and HrcQ appeared to be less efficient than the HrpB4–HrcD interaction in both assays, however, this might not necessarily reflect the in vivo situation when HrcQ is incorporated into the predicted sorting platform of the T3S system.

2.4 | The N-terminal cytoplasmic region of HrcD contributes to the interaction with HrpB4

HrcD is a putative IM ring protein with one transmembrane domain and an N-terminal cytoplasmic domain of approximately 120 amino acids (Berger et al., 2010; Hausner et al., 2019). Given its predicted function as IM ring component of the T3S system, HrcD presumably interacts with itself and the second IM ring component HrcJ as was reported for SctD and SctJ proteins from animal-pathogenic bacteria (Singh & Wagner, 2019). To test whether HrcD and HrcJ interact with themselves and with each other, we performed BACTH assays. As expected, we observed self-interactions of HrcD and HrcJ fusion proteins (Figure 4a). Furthermore, interactions between T18-HrcD and T25-HrcJ as well as between T18 fusions of HrcJ and T25-HrcD were detected, suggesting that HrcD and HrcJ interact with each other (Figure 4a).

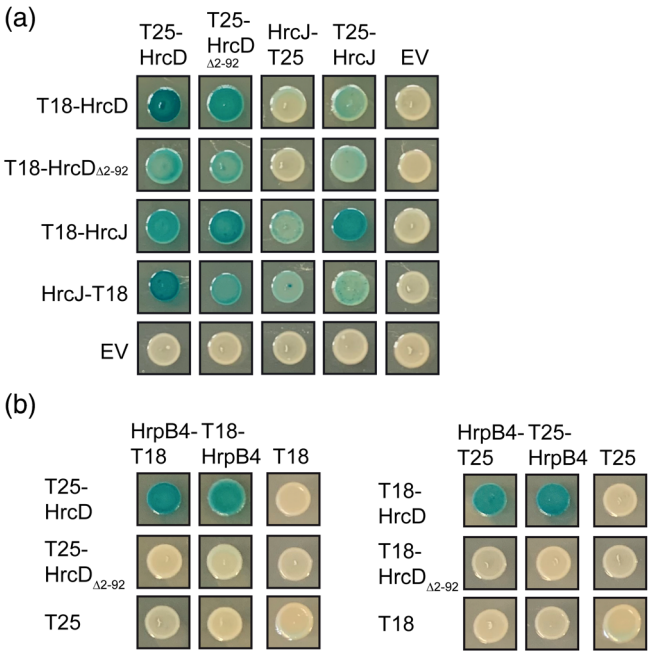

FIGURE 4 The cytoplasmic region of HrcD contributes to the interaction with HrpB4. (a) Interaction studies with HrcD and HrcJ. Expression constructs encoding T18 and T25 fusions of HrcD, HrcD$_{\Delta 2-92}$ and HrcJ as indicated were cotransformed into *E. coli* DHM1 cells, and bacterial cultures were grown on indicator plates. Photographs were taken after 3 days. EV, empty vector. (b) The cytoplasmic region of HrcD contributes to the interaction with HrpB4. Expression constructs encoding T18 and T25 fusions of HrpB4, HrcD and HrcD$_{\Delta 2-92}$ as indicated were cotransformed into *E. coli* DHM1 cells, and bacterial cultures were grown on indicator plates. Photographs were taken after 3 days

To investigate a possible contribution of the N-terminal cytoplasmic region of HrcD to protein–protein interactions, we performed additional interaction studies with an N-terminal HrcD derivative lacking amino acids 2–92 which are essential for protein function (Berger et al., 2010; Hausner et al., 2019). The results of BACTH assays suggest that HrcD$_{\Delta 2-92}$ self-interacts and interacts with HrcJ similarly to the full-length HrcD protein (Figure 4a). Notably, however, we did not observe an interaction between T25 and T18 fusions of HrcD$_{\Delta 2-92}$ with corresponding T18 and T25 fusions of HrpB4 (Figure 4b). The loss of detectable interaction between T18 fusions of HrpB4 and T25-HrcD$_{\Delta 2-92}$ was confirmed in the sensitive BTH101 reporter strain (Figure S6). These results were presumably not caused by a possible periplasmic localization of the N-terminal T25 or T18 fusion partners of HrcD$_{\Delta 2-92}$ because previous topology studies suggest that the cytoplasmic domain of HrcD spans approximately 120 amino acids (Berger et al., 2010; Hausner et al., 2019). Deletion of amino acids 2–92 should thus still result in the cytoplasmic localization of the N-terminal fusion partner. We, therefore, conclude that the cytoplasmic region of HrcD is dispensable for both self-interaction

and interaction with HrcJ but contributes to the interaction of HrcD with HrpB4.

2.5 | N- and C-terminal regions of HrpB4 contribute to the interaction with both HrcQ and HrcD as well as to pathogenicity

To investigate which regions of HrpB4 contribute to the interaction with HrcD and HrcQ, we performed interaction studies with HrpB4 derivatives deleted in the N- or C-terminal 30 amino acids. When analysed as T25 or T18 fusions by BACTH assays in *E. coli* DHM1 strains, HrpB4$_{\Delta 2-30}$ and HrpB4$_{\Delta C30}$ did not or not efficiently interact with corresponding T18 or T25 fusions of HrcD (Figure 5a). When tested in BTH101 cells, however, we detected an interaction between T18 fusions of HrpB4$_{\Delta 2-30}$ and T25-HrcD, suggesting that the interaction was not abolished in the absence of the N-terminal 30 amino acids of HrpB4 (Figure S6). No interactions between HrpB4 deletion derivatives and HrcQ fusions were detected in BTH101 strains (Figure 5b).

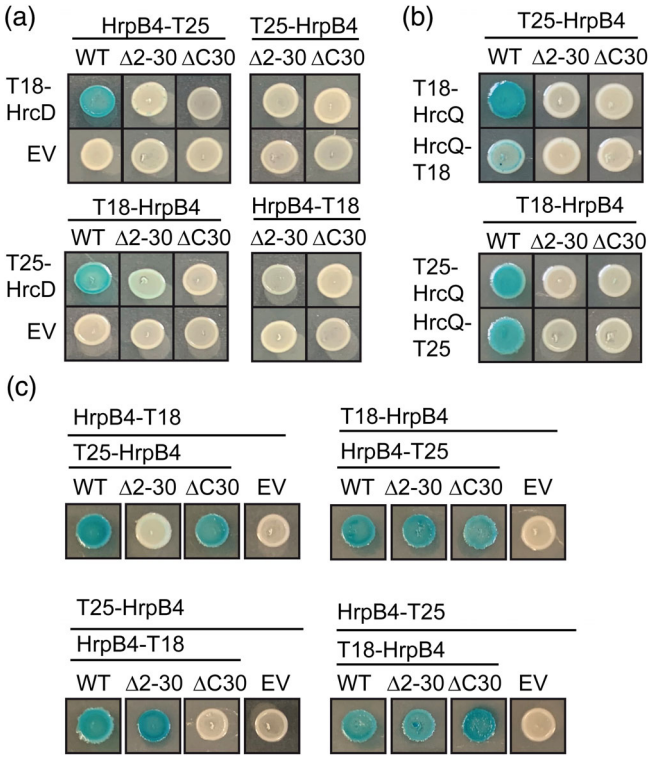

FIGURE 5 The N- and C-terminal regions of HrpB4 contribute to the interaction with HrcD and HrcQ but are dispensable for HrpB4 self-interaction. (a) The N- and C-terminal 30 amino acids of HrpB4 are required for the detectable interaction with HrcD. Expression constructs encoding T18 and T25 fusions of HrcD, HrpB4 (WT), HrpB4$_{\Delta 2-30}$ (Δ2–30) and HrpB4$_{\Delta C30}$ (ΔC30) were cotransformed into *E. coli* DHM1 cells as indicated. Bacterial cultures were grown on indicator plates and photographs were taken after 3 days. EV, empty vector. (b) HrpB4$_{\Delta 2-30}$ and HrpB4$_{\Delta C30}$ do not interact with HrcQ. Expression constructs encoding T18 and T25 fusions HrcQ, HrpB4 and derivatives thereof as indicated were cotransformed into *E. coli* BTH101 cells. Bacterial cultures were grown and photographed as described in (a). (c) The N- and C-terminal 30 amino acids are dispensable for HrpB4 self-interaction. Expression constructs encoding T18 and T25 fusions HrpB4 and deletion derivatives thereof as indicated were cotransformed into *E. coli* DHM1 cells. Bacterial cultures were grown and photographed as described in (a)

To investigate whether N- and C-terminal deletions in HrpB4 generally interfere with protein–protein interactions and thus with protein folding, we also tested a possible self-interaction of HrpB4 and deletion derivatives thereof. Using BACTH assays, we observed an interaction between HrpB4-T25 and T18-HrpB4 as well as between T25-HrpB4 and HrpB4-T18, suggesting a possible self-interaction of HrpB4 (Figure S6). Interactions were also observed with N- and C-terminal HrpB4 deletion derivatives, suggesting that the deletions did not interfere with HrpB4 self-interaction and thus presumably did not lead to a complete protein misfolding (Figure 5c).

To confirm the results of the BACTH assays, we investigated the interaction of GST-HrpB4 and deletion derivatives thereof with a C-terminally c-Myc epitope-tagged derivative of HrcD by GST pull-down assays. HrcD-c-Myc coeluted with GST-HrpB4 but was not or only weakly detectable in the eluates of N- and C-terminal deletion derivatives of GST-HrpB4 (Figure 6a). This confirms the above finding that deletions in the N- and C-terminal protein regions interfere with the interaction of HrpB4 with HrcD.

Next, we tested whether N- and C-terminal regions of HrpB4 are required for pathogenicity and introduced expression constructs encoding HrpB4-c-Myc and deletion derivatives thereof under control of the *lac* promoter into *hrpB4* deletion mutants which contained HrpG*. Complementation studies showed that deletion of the N-terminal 30 amino acids abolished the ability of HrpB4 to restore pathogenicity in the *hrpB4* mutant (Figure 6b). In contrast, deletion of the N-terminal 20 or the C-terminal 10 or 30 amino acids did not or only slightly interfere with the contribution of HrpB4 to pathogenicity (Figure 6b). Immunoblot analysis of bacterial cell extracts revealed that all HrpB4 deletion derivatives were synthesised (Figure 6b). Lack of complementation by HrpB4$_{\Delta 2-30}$-c-Myc was presumably not caused by a dominant-negative effect, because ectopic expression of the corresponding gene in the wild-type strain 85–10 did not significantly interfere with pathogenicity (Figure S7).

We also investigated whether the contribution of HrpB4 derivatives to pathogenicity was affected by the C-terminal c-Myc epitope or the overexpression from the *lac* promoter in the presence or absence of HrpG*. For this, *hrpB4* derivatives were expressed as untagged proteins under control of the native promoter in strain 85–10Δ*hrpB4* in the presence or absence of HrpG*. Infection experiments revealed that HrpB4$_{\Delta C10}$ partially complemented the *hrpB4* mutant phenotype in *hrpG* wild-type strains when expressed under control of the native promoter but was fully functional in the presence of HrpG* (Figure S7). No complementation was observed for HrpB4 derivatives lacking the N-terminal 20 or 30 amino acids or the C-terminal 30 amino acids when expressed under control of the native promoter in *hrpG* wild-type or *hrpG** strains (Figure S7). However, HrpB4$_{\Delta 2-20}$ and HrpB4$_{\Delta C30}$ were partially functional when analysed as C-terminally c-Myc epitope-tagged derivatives expressed under control of the *lac*

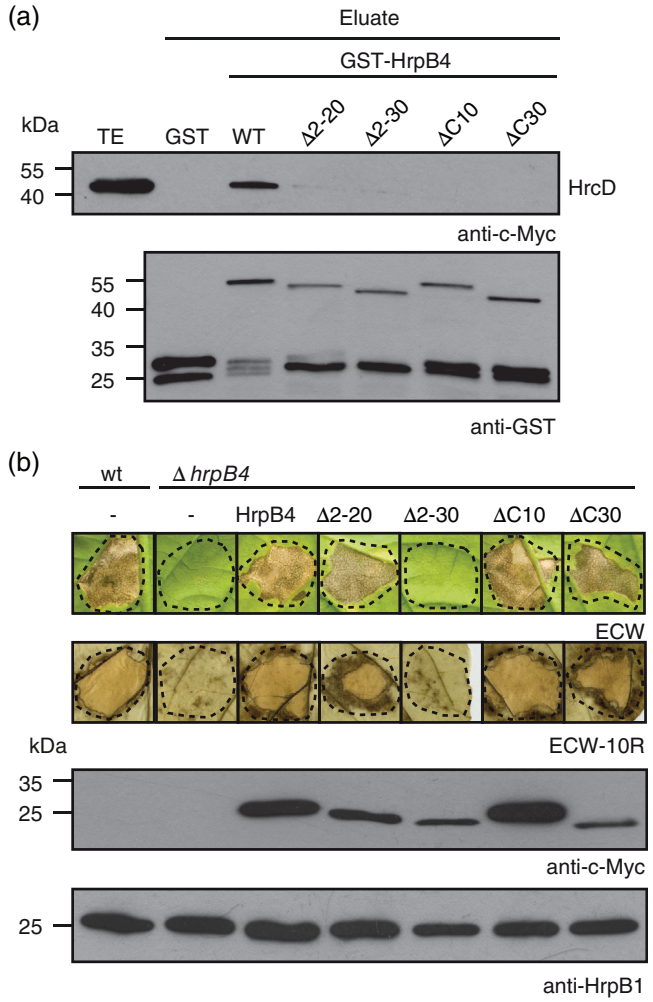

FIGURE 6 Analysis of HrpB4 deletion derivatives by in vitro interaction and in vivo complementation studies. (a) In vitro interaction studies with HrpB4 deletion derivatives and HrcD. GST, GST-HrpB4 and deletion derivatives thereof (GST-HrpB4$_{\Delta 2-20}$, GST-HrpB4$_{\Delta 2-30}$, GST-HrpB4$_{\Delta C10}$ and GST-HrpB4$_{\Delta C30}$) were immobilised on glutathione sepharose and incubated with a bacterial lysate containing HrcD-c-Myc. Total cell extracts (TE) and eluted proteins (eluates) were analysed by immunoblotting using c-Myc epitope- and GST-specific antibodies. (b) Complementation studies with HrpB4 deletion derivatives. *X. campestris* pv. *vesicatoria* strains 85–10 (wt) and 85–10Δ*hrpB4* (Δ*hrpB4*) containing HrpG* and expression constructs encoding HrpB4-c-Myc and derivatives thereof under control of the *lac* promoter and deleted in the N-terminal 20 (Δ2–20), 30 (Δ2–30) or C-terminal 10 (ΔC10) or 30 (ΔC30) amino acids as indicated were infiltrated into leaves of susceptible ECW and resistant ECW-10R pepper plants. Disease symptoms were photographed 9 dpi. For the better visualisation of the HR, leaves of resistant plants were destained in ethanol. Dashed lines indicate the infiltration sites. For protein analysis, bacterial cell extracts were analysed by immunoblotting using a c-Myc epitope-specific antibody. The blot was reprobed with a HrpB1-specific antibody to show equal loading

promoter in strain 85–10Δ*hrpB4* (Figure S7). Taken together, we conclude that deletion of the N- or C-terminal 30 amino acids interferes with the ability of HrpB4 to complement the *hrpB4* mutant phenotype.

2.6 | HrpB4 contributes to the formation of the predicted C ring

The interaction of HrpB4 with HrcQ and HrcD points to a possible role of HrpB4 as a linker between the predicted sorting platform and the IM rings of the T3S system. HrpB4 could thus act similarly to members of the SctK protein family from animal-pathogenic bacteria, which are required for the docking of the cytoplasmic sorting platform (Diepold et al., 2010; Hu, Lara-Tejero, Kong, Galan, & Liu, 2017; Tachiyama et al., 2019; Zhang et al., 2017). To investigate a contribution of HrpB4 to the association of HrcQ with the T3S system, we performed fluorescence microscopy studies with a HrcQ-sfGFP fusion protein which forms fluorescent foci in the presence of a functional T3S system (Hausner et al., 2019). For the analysis of HrcQ-sfGFP, we used an expression construct containing the modular T3S gene cluster without the native *hrcQ* gene which was assembled from individual modules corresponding to *hrp*, accessory and regulatory genes using Golden Gate cloning (Hausner et al., 2019). The modular design of the T3S gene cluster allowed the insertion of reporter fusions such as *hrcQ-sfgfp* as well as the removal of single genes or operons. The resulting constructs were introduced into the *hrp*-deficient *X. campestris* pv. *vesicatoria* strain 85*Δ*hrp*_fs*HAGX* which is deleted in the complete *hrp* gene cluster and contains additional mutations in regulatory (*hrpG*, *hrpX*) and accessory (*xopA*, *hpaH*) genes (Hausner et al., 2019). The accessory genes *xopA* and *hpaH* contribute to pathogenicity and are presumably required for efficient effector translocation and assembly of the T3S system in the periplasm, respectively (Hausner, Hartmann, Jordan, & Büttner, 2017; Noël, Thieme, Nennstiel, & Bonas, 2002). As reported previously, HrcQ-sfGFP was functional and complemented the *hrcQ* mutant phenotype (Figure 7a) (Hausner et al., 2019). To investigate a possible contribution of HrpB4 to HrcQ-sfGFP assembly, we introduced a frameshift mutation into *hrpB4* in the modular T3S gene cluster (Figure S8). As expected, bacteria containing the corresponding expression construct did not induce disease symptoms and the HR in susceptible and resistant pepper plants, respectively (Figure 7a). The mutant phenotype was complemented by an *sfgfp-hrpB4* expression cassette which was inserted into the flanking region of the T3S gene cluster and was generated for localization studies with HrpB4 (Figure 7a). Immunoblot analysis, however, revealed that sfGFP-HrpB4 was unstable, presumably resulting in the cleavage of sfGFP (data not shown). Thus, although being functional in terms of complementation of the *hrpB4* mutant phenotype, sfGFP-HrpB4 was not suitable for fluorescence microscopy analysis.

To study the localization of HrcQ-sfGFP in the absence of HrpB4, a modular T3S gene cluster with a deletion in *hrcQ*, a frameshift mutation in *hrpB4* and containing *hrcQ-sfgfp* was introduced into strain 85*Δ*hrp*_fs*HAGX*. As control, we used a modular T3S gene cluster deleted in the *hrpA* to *hpaB* operons which is deficient in T3S (Hausner et al., 2019). Immunoblot analysis confirmed that HrcQ-sfGFP was stably synthesised in all strains (Figure 7b). To study the localization of HrcQ-sfGFP, three transconjugands of each strain were grown under T3S-permissive conditions and inspected by fluorescence microscopy. As described previously, foci formation by HrcQ-sfGFP was abolished

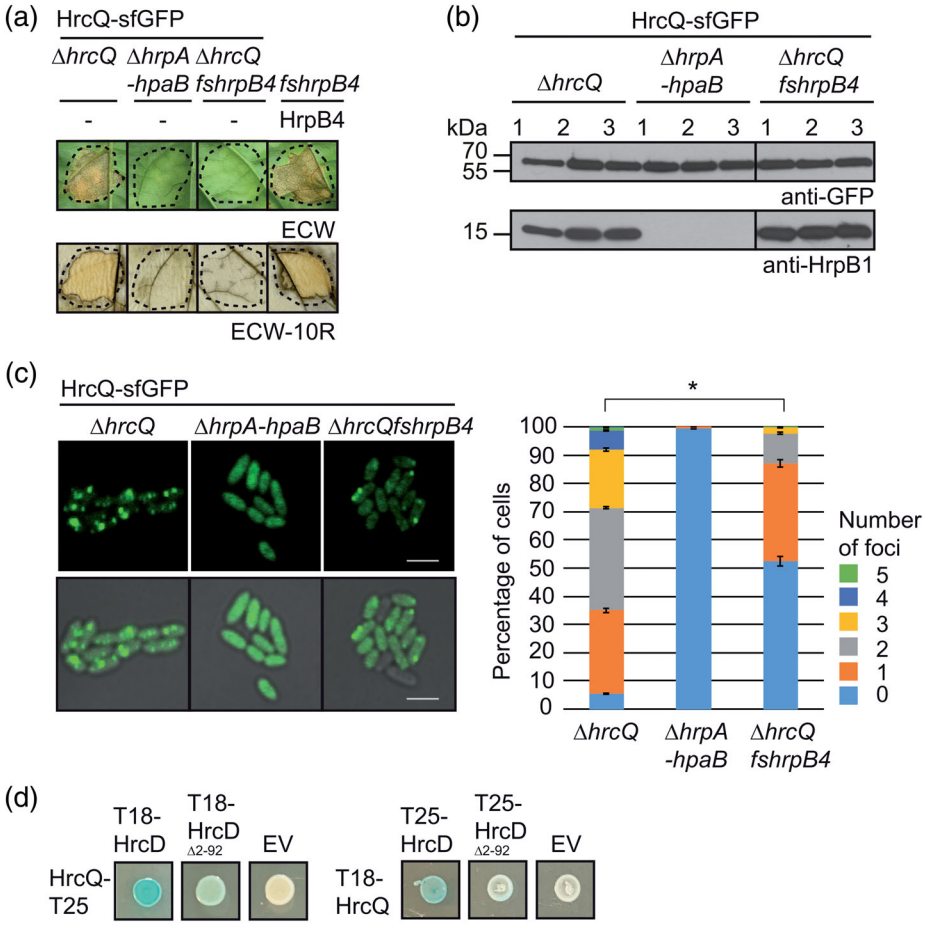

FIGURE 7 HrpB4 contributes to the formation of fluorescent foci by HrcQ-sfGFP. (a) A frameshift mutation in *hrpB4* in the modular T3S gene cluster abolishes pathogenicity of *X. campestris* pv. *vesicatoria*. Strain 85*Δ*hrp*_fs*HAGX* containing modular level P *hrp-HAGX* constructs encoding HrcQ-sfGFP and containing deletions in *hrcQ* (Δ*hrcQ*) or the *hrpA* to *hpaB* operons or containing a modular *hrp-HAGX* construct with a frameshift mutation in *hrpB4* in addition to the *hrcQ* deletion (Δ*hrcQ*fs*hrpB4*) as indicated was infiltrated into leaves of susceptible ECW and resistant ECW-10R pepper plants. For complementation studies, an *sfgfp-hrpB4* expression cassette (HrpB4) was inserted into the modular *hrp-HAGX* construct with the frameshift mutation in *hrpB4*. Disease symptoms were photographed 8 dpi. For the better visualisation of the HR, leaves of resistant plants were destained in ethanol. Dashed lines indicate the infiltration sites. (b) Immunological detection of HrcQ-sfGFP. Three transconjugands (labelled 1, 2, and 3) of strain 85*Δ*hrp*_fs*HAGX* encoding HrcQ-sfGFP on modular level P *hrp-HAGX* constructs with deletions in the *hrpA* – *hpaB* operons (Δ*hrpA-hpaB*), in *hrcQ* (Δ*hrcQ*), or with an additional frameshift mutation in *hrpB4* (Δ*hrcQ*fs*hrpB4*) as indicated were cultivated in minimal medium, and cell extracts were analysed by immunoblotting using antibodies specific for GFP and HrpB1. One representative blot probed with the anti-HrpB1 antibody is shown. (c) The mutation in *hrpB4* leads to a reduced number of fluorescent foci formed by HrcQ-sfGFP. Bacterial strains as described in (b) were incubated under T3S-permissive conditions and analysed by fluorescence microscopy. One representative image for every strain is shown. The size bar corresponds to 2 μm. The pictures in the lower panel result from an overlay of the signals from the fluorescence channel with the brightfield images. Fluorescent foci were counted in approximately 300 cells per strain in three transconjugands. Asterisks indicate a significant difference between the number of foci in strains with a p value < 0.05 based on the results of a χ^2 test. (d) Interaction studies with HrcQ and HrcD derivatives. Expression constructs encoding T18 and T25 fusions of HrcD, $HrcD_{\Delta 2-92}$ and HrcQ as indicated were cotransformed into *E. coli* BTH101 cells, and bacterial cultures were grown on indicator plates. Photographs were taken after 3 days. EV, empty vector

in the absence of the *hrpA* to *hpaB* operons (Hausner et al., 2019) (Figure 7c). The frameshift mutation in *hrpB4* significantly reduced the number of HrcQ-sfGFP foci when compared with the *hrpB4* wild-type strain, suggesting that HrpB4 contributes to but is not essential for the formation of HrcQ complexes and their association with the T3S system (Figure 7c). It is, therefore, possible that HrcQ complexes can also associate via the IM rings with the T3S system in the absence of HrpB4. To investigate a possible interaction of HrcQ with the IM ring protein HrcD, we performed BACTH assays with T25 and T18 fusions of HrcD and HrcQ. HrcQ interacted with HrcD when analysed as T25 or T18 fusion protein (Figure 7d). Notably, the interactions were only detected with the sensitive BTH101 reporter strain and were significantly reduced or abolished when HrcQ fusions were tested against the N-terminal HrcD deletion derivatives (Figure 7d and data not shown). This suggests that the N-terminal cytoplasmic domain of HrcD contributes to the interaction with HrcQ.

2.7 | The IM ring components HrcD and HrcJ are essential for the association of HrcQ-sfGFP with the T3S system

Given the interaction of HrcQ with the IM ring protein HrcD, we next analysed a potential influence of both IM ring components HrcD and HrcJ on HrcQ-sfGFP foci formation. For this, we generated modular T3S gene cluster constructs lacking in addition to *hrcQ* either *hrcD* or *hrcJ* (Figure S8). As expected, deletion of *hrcD* or *hrcJ* led to a loss of pathogenicity when the corresponding constructs were analysed in strain 85*Δ*hrp*_fs*HAGX* (Figure 8a). Insertion of an *sfgfp-hrcD* or *sfgfp-hrcJ* expression cassette into the flanking region of the corresponding modular T3S gene cluster constructs restored the wild-type phenotype, suggesting that the loss of pathogenicity was caused by the absence of HrcD and HrcJ, respectively, and not by a polar effect of the deletions on flanking genes (Figure 8a). As already observed for sfGFP-HrpB4, sfGFP-HrcD and sfGFP-HrcJ fusion proteins were unstable leading to the cleavage of the sfGFP fusion partner and could, therefore, not be used for localization studies (data not shown).

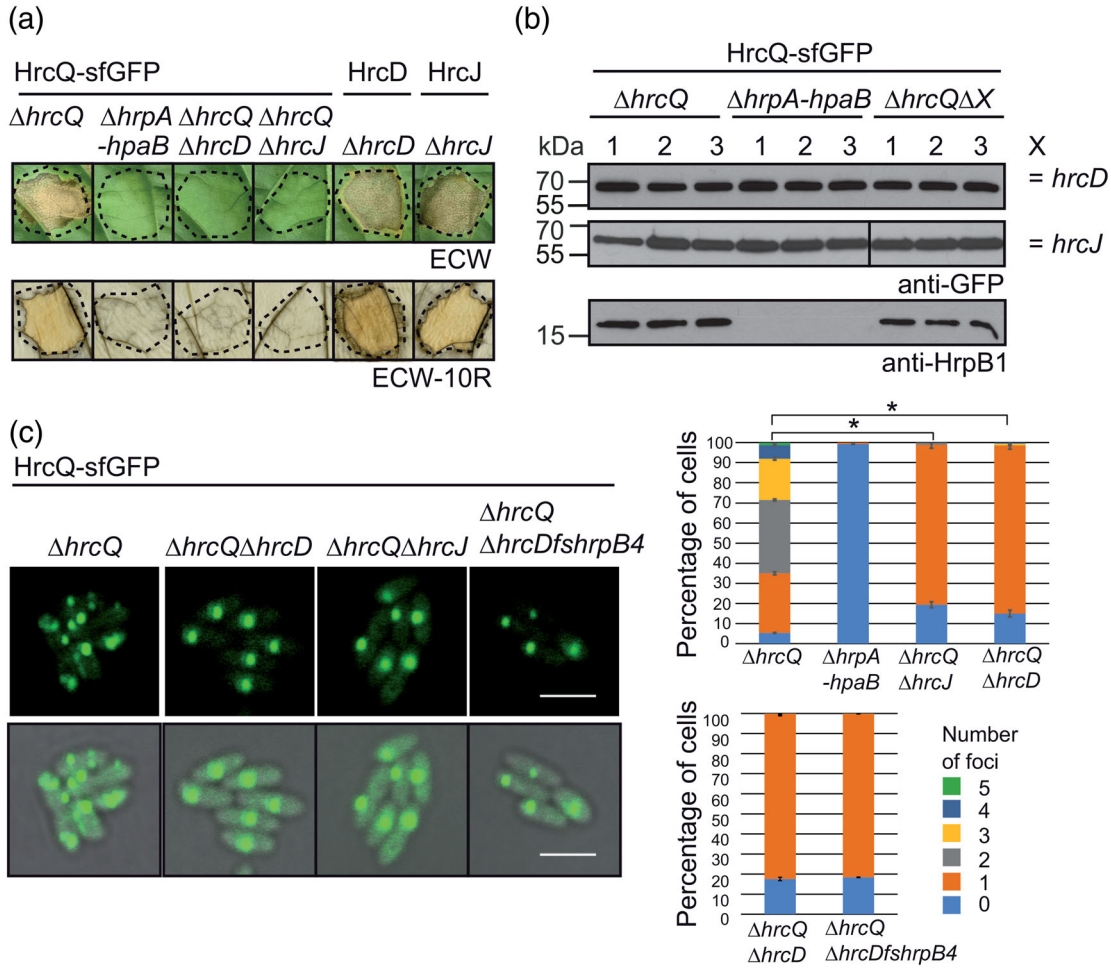

FIGURE 8 Fluorescent foci formation by HrcQ-sfGFP is severely reduced in the absence of the IM ring components HrcD and HrcJ. (a) Complementation studies with *hrcD* and *hrcJ* mutants. For complementation studies, strain 85*Δ*hrp*_fs*HAGX* containing modular level P *hrp-HAGX* constructs encoding sfGFP-HrcD (HrcD) or sfGFP-HrcJ (HrcJ) and containing deletions in *hrcD* or *hrcJ* as indicated was used. Additionally, strain 85*Δ*hrp*_fs*HAGX* containing modular level P *hrp-HAGX* constructs encoding HrcQ-sfGFP and containing deletions in *hrcQ* (Δ*hrcQ*), the *hrpA* to *hpaB* operons (Δ*hrpA-hpaB*), *hrcQ* and *hrcD* (Δ*hrcQ*Δ*hrcD*) or *hrcQ* and *hrcJ* (Δ*hrcQ*Δ*hrcJ*) as indicated was used for the infection experiments. Bacteria were infiltrated into leaves of susceptible ECW and resistant ECW-10R pepper plants. Disease symptoms were photographed 9 dpi. For the better visualisation of the HR, leaves of resistant plants were destained in ethanol. Dashed lines indicate the infiltration sites. (b) Immunological detection of HrcQ-sfGFP. Three transconjugands (labelled 1, 2, and 3) of strain 85*Δ*hrp*_fs*HAGX* encoding HrcQ-sfGFP on modular level P *hrp-HAGX* constructs with mutations in *hrcQ* (Δ*hrcQ*), the *hrpA* – *hpaB* operons (Δ*hrpA-hpaB*), *hrcD* (Δ*hrcD*) or *hrcJ* (Δ*hrcJ*) as indicated were cultivated in minimal medium and cell extracts were analysed by immunoblotting using antibodies specific for GFP and HrpB1, respectively. (c) HrcD and HrcJ contribute to foci formation by HrcQ-sfGFP. Bacterial strains as described in (b) were incubated under T3S-permissive conditions and analysed by fluorescence microscopy. One representative image for every strain is shown. The size bar corresponds to 2 μm. The pictures in the lower panel result from an overlay of the signals from the fluorescence channel with the brightfield images. Fluorescent foci were counted in approximately 300 cells per strain in three transconjugands. Asterisks indicate a significant difference between the number of foci in strains with a p value < 0.05 based on the results of a χ^2 test

HrcQ-sfGFP, however, was stably synthesised in comparable amounts in all strains (Figure 8b).

For localization studies, bacteria were grown under T3S-permissive conditions and inspected by fluorescence microscopy as described above. In the absence of HrcD or HrcJ, HrcQ-sfGFP formed only one bright fluorescent spot per cell (Figure 8c), suggesting that the deletion of either *hrcD* or *hrcJ* abolished the association of HrcQ-sfGFP with the T3S system and led to a cytoplasmic accumulation of HrcQ-sfGFP. The HrcQ-sfGFP complexes in *hrcD* and *hrcJ* mutants might correspond to the predicted sorting platform, which presumably assembles in the cytoplasm in the absence of the IM rings. To investigate whether HrpB4 contributes to the formation of HrcQ-sfGFP complexes in the cytoplasm, we generated an additional modular T3S gene cluster construct with mutations in *hrcQ* and both *hrcD* and *hrpB4* (Figure S8). Notably, however, additional mutation of *hrpB4* in the *hrcD* deletion mutant did not detectably alter foci formation by HrcQ-sfGFP (Figure 8c). We, therefore, conclude that HrpB4 contributes to the association of HrcQ-sfGFP with the T3S system but is not required for the assembly of fluorescent HrcQ-sfGFP complexes in the cytoplasm in the absence of the IM ring component HrcD.

3 | DISCUSSION

HrpB4 is an essential pathogenicity factor from *X. campestris* pv. *vesicatoria* and is homologous to HrpB4 proteins from *Xanthomonas* spp. and *R. solancearum* (Rossier et al., 2000). Our finding that HrpB4 from *X. campestris pv. campestris* complements the *hrpB4* mutant phenotype in *X. campestris* pv. *vesicatoria* suggests that HrpB4 proteins are functionally interchangeable despite the differences in their amino acid sequences (Figure 1). Comparative sequence analyses revealed that the sequence diversity mainly occurs within the N-terminal 90 amino acids, however, similar secondary structures are predicted for both proteins (Figure S9). HrpB4 is encoded between *hrcJ* and *hrcL* in the *hrp* gene cluster of *X. campestris* pv. *vesicatoria* and thus shares a similar genetic localization with *sctK* genes from animal-pathogenic bacteria which are often located between *sctJ* and *sctL* in the T3S gene clusters (Figure 1a) (Soto et al., 2017). SctK proteins including, for example, MxiK from *Shigella flexneri*, OrgA from *Salmonella* spp., PscK from *Pseudomonas aeruginosa* and YscK from *Yersinia* spp. are highly sequence diverse and act as linkers between the IM ring and the sorting platform of the T3S system (Lara-Tejero, 2019; Muthuramalingam et al., 2020; Soto et al., 2017).

In the present study, we show that HrpB4 is a soluble protein and associates with the bacterial membranes independently of the T3S system (Figure 2). A similar T3S system-independent membrane localization was previously described for EscK from *E. coli* as well as for HrpB7 from *X. campestris* pv. *vesicatoria* which is a predicted member of the HrpO/FliJ/YscO family and associates with the IM and predicted C ring components (Drehkopf, Otten, Hausner, Seifert, & Büttner, 2020; Soto et al., 2017). The results of our in vivo and in vitro interaction studies revealed that HrpB4 interacts with the putative C ring protein HrcQ, which is homologous to SctQ proteins from animal-pathogenic bacteria and might thus be part of the predicted sorting platform of the T3S system (Figure 3). The interaction between HrpB4 and HrcQ was detected by both BACTH and GST pull-down assays and appeared to be relatively weak. It remains to be investigated whether both proteins interact more efficiently when incorporated into the predicted sorting platform of the T3S system in *X. campestris* pv. *vesicatoria*.

In animal-pathogenic bacteria, SctQ proteins form six pod-like structures which are each connected through a single SctK protein to the cytoplasmic domains of the IM ring component SctD (Diepold et al., 2017; Hu et al., 2017; Tachiyama et al., 2019). In plant-pathogenic bacteria, however, the presence of a sorting platform is still enigmatic. We previously showed that HrcQ assembles into complexes and associates with the ATPase HrcN and its predicted regulator HrcL (Lorenz et al., 2012; Lorenz & Büttner, 2009). Furthermore, fluorescence microscopy studies revealed that HrcQ-sfGFP forms fluorescent foci suggesting that HrcQ is a component of an oligomeric protein complex (Hausner et al., 2019). As no HrcQ-sfGFP foci are detected in the absence of the T3S system, HrcQ complex formation likely depends on additional components of the secretion apparatus (Hausner et al., 2019).

In the present study, fluorescence microscopy analyses showed that the number of HrcQ-sfGFP foci was severely reduced in the absence of HrpB4 (Figure 7). This is in agreement with the predicted role of HrpB4 as a linker between the putative sorting platform and the IM ring. Notably, however, foci formation by HrcQ-sfGFP was not completely abolished in *hrpB4* mutants, suggesting a residual docking of HrcQ-containing complexes to the T3S system in the absence of HrpB4 (Figure 7). This hypothesis will be confirmed in future studies by colocalization of HrcQ-sfGFP with an integral membrane component of the T3S system. However, given that the cytoplasmic localization of HrcQ-sfGFP would likely not result in the formation of distinct foci, we assume that HrpB4 contributes to but is not essential for the association of HrcQ-containing protein complexes with the membrane-spanning secretion apparatus. This is in contrast to the role of most SctK proteins from animal-pathogenic bacteria, which are essential for the formation of the sorting platform. For example, in *Salmonella* spp., the absence of the SctK protein OrgA leads to a relocalization of a fluorescent fusion of the SctQ protein SpaO to the bacterial cytoplasm resulting in a complete loss of foci formation and the disappearance of the sorting platform at the T3S system (Hu et al., 2017; Zhang et al., 2017). A similar essential contribution to the assembly of the sorting platform was described for the SctK proteins MxiK from *S. flexneri* and YscK from *Yersinia* spp. (Diepold et al., 2010;Hu et al., 2017 ; Tachiyama et al., 2019). Given the role of the sorting platform as T3S substrate acceptor site, the loss of SctK presumably prevents the recruitment of T3S substrates. In *E. coli*, the T3S defect in the absence of the SctK protein EscK can be overcome by overproduction of T3S substrates (Soto et al., 2017). It was, therefore, speculated that EscQ structures occasionally associate with the T3S system in the absence of EscK, thus allowing weak T3S (Soto et al., 2017). In *X. campestris* pv. *vesicatoria*, however, overproduction of T3S genes or ectopic expression of single effectors in the *hrpB4* deletion mutant did not restore pathogenicity or effector protein translocation (Figure 1;

data not shown). Furthermore, the *hrpB4* deletion mutant phenotype was not complemented by overexpression of *hrcQ*, suggesting that the lack of HrpB4 cannot be compensated by increased levels of HrcQ or T3S substrates (data not shown).

It remains to be investigated whether the residual foci formation by HrcQ-sfGFP in *hrpB4* mutants results from the docking of HrcQ to the T3S system via HrcD or the ATPase complex. We have previously shown that HrcQ interacts with the ATPase HrcN and its predicted regulator HrcL (Lorenz et al., 2012). HrcQ and HrcN both interact with the predicted coiled-coil protein HrpB7, which is a member of the HrpO/FliJ/YscO family and also binds to the IM ring of the T3S system (Drehkopf et al., 2020) (Figure 9). However, HrpB7 presumably does not act as an essential linker between the sorting platform and the membrane-spanning secretion apparatus because it is dispensable for the formation of fluorescent HrcQ-sfGFP foci (Drehkopf et al., 2020). In future experiments, we will, therefore, analyse the contribution of the ATPase complex to HrcQ-sfGFP localization in wild-type and *hrpB4* mutant strains. In addition to the ATPase complex, HrcQ might directly interact with the IM rings in the absence of HrpB4. Notably, we detected an interaction between HrcQ and the IM ring protein HrcD when both proteins were analysed using BACTH assays (Figure 7). Furthermore, the analysis of HrcQ-sfGFP in *hrcD* and *hrcJ* mutants revealed that the IM rings are essential for the docking of HrcQ complexes to the T3S system. Thus, HrcQ-sfGFP formed large fluorescent clusters in the bacterial cytoplasm of *hrcD* and *hrcJ* mutants (Figure 8). A similar aggregation was reported for a fluorescent fusion of the SctQ protein SpaO in *Salmonella* mutants lacking the IM rings, the inner rod and the needle (Zhang et al., 2017). Cytoplasmic SctQ proteins from animal-pathogenic bacteria might be part of fully or partially assembled sorting platforms as was suggested for *Salmonella* spp. and *Yersinia* spp. (Diepold et al., 2017; Rocha et al., 2018; Zhang et al., 2017). In *X. campestris* pv. *vesicatoria*, the additional mutation of *hrpB4* in a *hrcD* mutant did not alter the localization pattern of HrcQ-sfGFP, suggesting that HrpB4 is dispensable for the stabilisation of HrcQ-sfGFP complexes in the cytoplasm. In agreement with this observation, immunoblot analysis of bacterial cell extracts did not reveal a contribution of HrpB4 to HrcQ stability and vice versa (data not shown). Given the cytoplasmic and membrane-associated localization of HrpB4, we speculate that it is a component of the predicted cytoplasmic sorting platform and can, therefore, dissociate from the membrane-spanning secretion apparatus as proposed for SctK proteins from animal-pathogenic bacteria (Diepold et al., 2010; Diepold et al., 2017) (Figure 9).

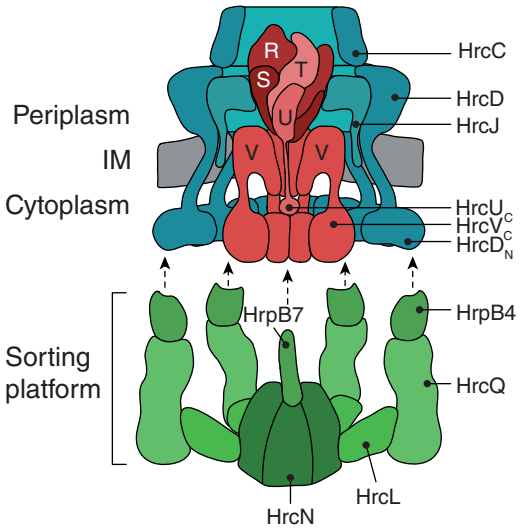

FIGURE 9 Model of the predicted sorting platform and IM-associated components of the T3S system from *X. campestris* pv. *vesicatoria*. Components of the export apparatus including HrcR, HrcS and HrcT (R, S, T) in the periplasm and the transmembrane proteins HrcU and HrcV (U, V) are show in red. HrcU and HrcV contain large cytoplasmic domains (HrcU$_C$ and HrcV$_C$). The export apparatus is embedded in the IM rings which consist of HrcJ and HrcD. The N-terminal cytoplasmic domain of HrcD (HrcD$_N$) interacts with the linker protein HrpB4, which is likely a component of the predicted sorting platform. HrpB4 interacts with HrcQ, which presumably forms six pod-like structures and is linked via HrcL with the hexameric ATPase HrcN. The predicted coiled-coil protein HrpB7 interacts with the ATPase and the IM rings. See text for details. The IM is shown in grey, components of the predicted sorting platform in green

In agreement with the proposed function of HrpB4 as a linker protein, we identified the predicted IM ring component HrcD as additional HrpB4 interaction partner (Figure 3). HrcD belongs to the SctD family of IM ring components which have not yet been functionally characterised in *X. campestris* pv. *vesicatoria*. In the present study, BACTH assays showed that HrcD interacts with itself and the predicted second IM ring component HrcJ as expected, suggesting that both proteins are part of a heterooligomeric protein complex (Figure 4). Previous topology studies revealed that HrcD contains a transmembrane domain and an N-terminal cytoplasmic region which spans approximately 120 amino acids and is essential for HrcD function (Berger et al., 2010; Hausner et al., 2019). In the present study, we show that the N-terminal 92 amino acids are dispensable for the self-interaction of HrcD and its interaction with HrcJ. Notably, however, deletion of the N-terminal 92 amino acids in HrcD abolished the detectable interaction with HrpB4, suggesting that HrpB4 interacts with the cytoplasmic domain of HrcD (Figure 4). Similar results were reported for the SctK proteins OrgA from *Salmonella typhimurium* and MxiK from *S. flexneri* which interact with or are located in close proximity to the cytoplasmic domains of SctD proteins (Hu et al., 2017; Tachiyama et al., 2019).

The interaction of HrpB4 with both HrcD and HrcQ confirms the predicted role of HrpB4 as a linker between the IM ring and the putative sorting platform. Notably, we did not detect interactions between HrpB4 and the second IM ring component HrcJ or components of the ATPase complex, suggesting that HrpB4 does not generally interact with cytoplasmic components of the T3S system (Figure 3). Interaction and complementation studies revealed that the N- and C-terminal 30 amino acids of HrpB4 contribute to its interaction with HrcD and HrcQ as well as to pathogenicity. Notably, no interaction with HrcD and HrcQ was detectable for HrpB4$_{\Delta C30}$, yet, this deletion derivative was still partially functional. Given the predicted role of HrpB4 as a linker between HrcQ and HrcD, we assume that the deletion did not completely abolish the interaction of HrpB4 with HrcQ and HrcD in vivo. Structural studies with HrpB4 proteins might help to investigate whether the N- and C-terminal

regions of HrpB4 are located in a protein region which contributes to the interaction of HrpB4 with different interaction partners. Notably, the N- and C-terminal regions of the SctK protein PscK from *P. aeruginosa* are located in close proximity to each other as was recently revealed by crystal structure analysis (Muthuramalingam et al., 2020). Furthermore, a single region in the SctK protein MxiK from *S. flexneri* was reported to be involved in the interaction of MxiK with both Spa33 (SctQ) and the cytoplasmic region of MxiG (SctD) (Tachiyama et al., 2019). In future studies, we will generate additional HrpB4 mutant derivatives to more accurately localise HrcQ and HrcD binding sites and to minimise a potential negative effect of the mutations on HrpB4 folding. Computational analyses suggested that the deletion of the N-terminal 30 amino acids did not significantly affect the predicted secondary structure (Figure S9). Furthermore, we observed that HrpB4 as well as N- and C-terminal deletion derivatives thereof interact with each other, suggesting that the deletions did not lead to a complete protein misfolding (Figure 5). It remains to be investigated whether the self-interaction of HrpB4 contributes to its role during T3S.

Taken together, our data suggest that HrpB4 acts similarly to SctK proteins which have not yet been studied in plant-pathogenic bacteria. In contrast to the essential role of SctK family members as linker proteins in animal-pathogenic bacteria, HrpB4 is not essential for the formation of HrcQ complexes in *X. campestris* pv. *vesicatoria*. Given the essential contribution of HrpB4 to pathogenicity, we assume that the residual assembly of HrcQ-sfGFP complexes in *hrpB4* mutants is not sufficient to promote T3S. It is, therefore, possible that HrpB4 is required for the formation of a functional sorting platform. Future studies will focus on the elucidation of the predicted role of HrpB4 to the assembly of components of the predicted sorting platform including the ATPase complex.

4 | MATERIAL AND METHODS

4.1 | Bacterial strains and growth conditions

Bacterial strains and plasmids are listed in Table S1. *E. coli* strains were cultivated at 37°C in lysogeny broth (LB) medium and *X. campestris* pv. *vesicatoria* strains at 30°C in nutrient-yeast extract-glycerol (NYG) medium (Daniels, Barber, Turner, Cleary, & Sawczyc, 1984). For T3S assays, we used minimal medium A (MA) supplemented with sucrose (10 mM) and casamino acids (0.3%) (Ausubel et al., 1996). Plasmids were introduced into *E. coli* and *X. campestris* pv. *vesicatoria* by electroporation. Antibiotics were added to the media at the following final concentrations: ampicillin, 100 μg/mL; kanamycin, 25 μg/mL; rifampicin, 100 μg/mL; spectinomycin, 100 μg/mL, gentamycin, 15 μg/mL; streptomycin, 25 μg/mL and nalidixic acid, 15 μg/mL.

4.2 | Plant material and plant infections

Infection studies were performed with the near-isogenic pepper cultivars Early Cal Wonder (ECW) and ECW-10R (Kousik & Ritchie, 1998; Minsavage et al., 1990). *X. campestris pv. vesicatoria* strains were infiltrated with a needle-less syringe into leaves at concentrations of 1×10^8 colony forming units (CFU)/mL in 1 mM $MgCl_2$ if not stated otherwise. Infected pepper plants were incubated for 16 h of light at 28°C and 65% humidity, and 8 h of darkness at 22°C and 65% humidity. Plant reactions were observed over a period of one to ten dpi. Leaves of resistant plants were destained in 70% ethanol for a better visualisation of the HR. Infection experiments were performed at least three times with different transconjugants. Representative results are shown.

4.3 | Generation of expression constructs

To generate *hrpB4* and *hrcJ* expression constructs, genes were amplified by PCR from DNA of *X. campestris pv. vesicatoria* strain 85–10 or *X. campestris pv. campestris* strain 8004, and subcloned as blunt-end fragments using SmaI and ligase into vector pICH41021. Inserts were subsequently ligated into the BsaI sites of vector pBRM, downstream of a *lac* promoter and in frame with a C-terminal 3 x c-Myc epitope-encoding sequence using Golden Gate cloning (Engler, Kandzia, & Marillonnet, 2008). Additionally, *hrpB4* and the promoter of the *hrpB* operon were cloned into vector pBRM-P-stop, which contains a stop codon upstream of the 3 x c-Myc epitope-encoding sequence, resulting in the synthesis of untagged HrpB4 under control of the native promoter. For the generation of N- and C-terminal deletion derivatives of HrpB4, we amplified the corresponding gene regions by PCR from plasmid pBhrpB4 and subsequently inserted the amplicons into vector pICH41021 using SmaI and ligase.

hrpB4$_{\Delta 2-20}$ was subcloned into pAGM9121 using the type IIs enzyme BpiI and ligase. The corresponding inserts were subsequently ligated into vector pBRM or in combination with the *hrpB* operon promoter into vector pBRM-P, thus resulting in expression constructs encoding HrpB4$_{\Delta 2-20}$, HrpB4$_{\Delta 2-30}$, HrpB4$_{\Delta C10}$ and HrpB4$_{\Delta C30}$ as untagged derivatives under control of the native promoter or as C-terminally c-Myc epitope-tagged derivatives under control of the *lac* promoter. To generate GST-HrpB4 expression constructs, modules corresponding to *hrpB4* or deletion derivatives thereof and *ptac-gst* (encodes GST under control of the *ptac* promoter) were cloned into vector pBRM-P-stop. All constructs are listed in Table S1.

4.4 | Modification of BACTH vectors for Golden Gate cloning and generation of expression constructs for BACTH assays

The BACTH vectors pKT25, pKNT25, pUT18 and pUT18C (Euromedex) (Karimova et al., 2001), which encode T18 and T25 fragments of CyaA, were modified to allow Golden Gate cloning of genes of interest and the generation of T18 and T25 fusion proteins in fusion with a FLAG epitope for immunodetection. For this, we replaced the original mcs of the vectors by a cassette encoding the eforRed chromoprotein as selection marker downstream of a *lac* promoter. The *plac-eforRed* cassette was amplified by PCR using primers

eforRed-TATG-F and eforRed-GGTG-R and was flanked by BsaI sites generating upstream 5′-TATG-3′ and downstream 5′-GGTG-3′ overhangs. For the generation of the Golden Gate-compatible vectors $pKT25_{GG}$ and $pKNT25_{GG}$, the vector backbones of the original vectors pKT25 and pKNT25 without the mcs were amplified by PCR using the primer pairs pKTmod-GGTG-F/T25-TATG-FLAG-R (for pKT25) and T25-GGTG-FLAG-F/pUTmod-TATG-R (for pKNT25) and assembled with the *eforRed* gene using BpiI and ligase (Figure S4). The primer sequences introduced a FLAG epitope-encoding sequence, which was inserted between the CyaA fragment-encoding genes and the *lacP-eforRed* cassette, as shown in Figure 3a.

For the generation of the Golden Gate-compatible vectors $pUT18_{GG}$ and $pUT18C_{GG}$, the *plac-eforRed* cassette was amplified as described above and assembled with modified vector fragments and a gentamycin resistance cassette which was amplified using primers GentR-TGTG-F/GentR-CTGT-R. We replaced the original ampicillin resistance cassette of both vectors by a gentamycin resistance cassette to facilitate the selection of positive clones after Golden Gate cloning because most genes of interest were first subcloned into a cloning vector containing an ampicillin resistance gene. To generate $pUT18_{GG}$, part of the original pUT18 vector containing the origin of replication was amplified using primers pUTmod-res-CTGT-F and pUTmod-TATG-R. The T18-encoding fragment was amplified with the primer pair T18-GGTG-FLAG-F and pUTmod-res-ACAC-R (Figure S4). The resulting fragments, the *eforRed* and the gentamycin resistance gene were assembled using BpiI and ligase, thus resulting in vector $pUT18_{GG}$. Similarly, for the generation of $pUT18C_{GG}$, vector fragments were amplified by PCR using the primer pairs pUTmod-res-CTGT-F/T18-TATG-FLAG-R and pUTmod-GGTG-F/pUTmod-res-ACAC-R, and assembled with the gentamycin resistance gene and the *eforRed* cassette, as described above (Figure S4). Due to the presence of a BpiI site in the T18-encoding sequence, an additional ligation step was performed after Golden Gate assembly. All primer sequences are listed in Table S2. The positions of the primers used for the generation of the modified BACTH vectors is summarised in Figure S4. For the generation of expression constructs encoding T18 or T25 fusion proteins, genes or gene fragments were cloned into the BsaI sites of vectors $pKT25_{GG}$, $pKNT25_{GG}$, $pUT18_{GG}$ and $pUT18C_{GG}$ by Golden Gate cloning. All constructs are listed in Table S1.

4.5 | Generation of modular T3S gene cluster constructs for the analysis of HrcQ-sfGFP

Modular T3S gene cluster constructs were generated as described previously and are summarised in Figure S8 (Hausner et al., 2019). The frameshift mutation in *hrpB4* was inserted by amplifying *hrpB4* with primers FShrpB4-MoClo-F and hrpB4-MoClo-R using the level-2 construct pAGB191 as a template. The frameshift mutation leads to the generation of a stop codon after codon 54 of *hrpB4*. The amplicon was cloned into the pAGM9121 vector using BpiI and ligase, thus generating the level-2 construct pAGB770. In a next cloning step, *hrpB1* to *hrpB4* of the *hrpB* operon were assembled from constructs pAGB770 (*hrpB4*fs), the level-2 constructs pAGB187 (native *hrpB* operon promoter; *phrpB*), pAGB188 (*hrpB1*), pAGB189 (*hrpB2*) and pAGB190 (*hrcJ*) in the level-1 vector pAGM1311 using BsaI and ligase. The insert of the resulting construct pAGB776 was subsequently assembled with the level-1 module from construct pAGB198, which contains *hrcL* to *hrcT* and *hrcC*, in the level 0 vector pICH41331 using BpiI and ligase, thus generating construct pAGB782 (corresponding to the *hrpA* and *hrpB* operons with a frameshift mutation in *hrpB4*). The insert of pAGB782 was then cloned using BsaI and ligase into the level 1 destination vector pICH47811, resulting in construct pAGB788. The whole *hrp* gene cluster was assembled in the level M vector pAGM8031 using BpiI and ligase from construct pAGB788, the additional level 1 constructs pAGB275 (*hrpC-hpaB* operons; Δ*hrcQ*) and pAGB156 (*hrpF* operon), the dummy module pICH54022 and the end linker pICH50900, thus generating the level M construct pAGB794.

For the deletion of *hrcJ* in the modular T3S gene cluster, construct pAGB190 (*hrcJ*) was amplified using the phosphorylated primers P-hrcJ-N-MoClo-F/P-hrcJ-N-MoClo-R, which introduced the deletion in *hrcJ*. The amplicon was ligated, thus resulting in construct pAGB516 (Δ*hrcJ*). The subsequent assembly of the inserts of constructs pAGB516 (Δ*hrcJ*), pAGB187, pAGB188, pAGB189 and pAGB191 (*hrpB4*) in vector pAGM1311 using BsaI and ligase led to level-1 construct pAGB675 (*hrpB1-hrpB4* with a deletion in *hrcJ*). The inserts of constructs pAGB675 and pAGB198 (*hrcL* to *hrcT* including *hrcC*) were subsequently assembled in vector pICH41221 using BpiI and ligase, thus leading to level 0 construct pAGB679 (*hrpA* and *hrpB* operons with a deletion in *hrcJ*). The insert of construct pAGB679 was transferred into the level 1 destination vector pICH47811 using BsaI and ligase, resulting in construct pAGB682. The whole T3S gene cluster was subsequently assembled in vector pAGM8031 using BpiI and ligase and constructs pAGB682, pAGB275 (*hrpC* to *hpaB* operons with a deletion in *hrcQ*), pAGB156 (*hrpF* operon), the dummy module construct pICH54022 and the end linker-containing vector pICH50900, thus generating level M construct pAGB763.

For the introduction of a deletion in *hrcD*, the level-2 construct pAGB206 (containing *hpaA* and *hrcD*) was used as template for PCR reactions with primer pairs hrcD-DELMoClo-F1/hrcD-DELMoClo-R1, hrcD-DELMoClo-F2/hrcD-DELMoClo-R2 and hrcD_DELMoClo_F3/hrcD-DELMoClo-R3. The resulting amplicons contained *hpaA* as well as 5′ and 3′ regions of *hrcD* flanking the deletion. Amplicons were cloned into vector pAGM9121, using BpiI and ligase thus generating the level-2 construct pAGB259. The corresponding insert was subsequently assembled with inserts from constructs pAGB205 (containing *hrcS*), pAGB207 (containing *hrpD6*), pAGB208 (containing *hrpE* and *hpaB*) and pAGB209 (*hpaE*) into pAGM1311, using BsaI and ligase and leading to the level-1 construct pAGB261. The inserts of constructs pAGB261, pAGB272 (contains the *hrpC* operon including the promoter, the native promoter of the *hrpD* operon with a deletion in *hrcQ* and the *hrcR* gene) were assembled in level 0 vector pICH41331 using BpiI and ligase and generating the level 0 construct pAGB869. The insert of pAGB869 was transferred to level 1 vector pICH47751

using BsaI and ligase, resulting in the level 1 construct pAGB870. The inserts of constructs pAGB870 and pAGB275 (*hrpC* to *hpaB* operons with a deletion in *hrcQ*) and pAGB156 (contains *hrpF*) were assembled in vector pAGM8031, thus resulting in the level M construct pAGB871 which contains the complete *hrp* gene cluster with deletions in *hrcD* and *hrcQ*. For the simultaneous introduction of the deletion in *hrcD* and the frameshift mutation in *hrpB4*, the inserts of constructs pAGB788 (*hrpA* to *hrpB* operons with a frameshift mutation in *hrpB4*), pAGB870 (*hrpC* to *hpaB* operons with deletions in *hrcQ* and *hrcD*), pAGB156 (*hrpF* operon), pICH54022 (dummy module) and pICH50900 (end linker) were assembled using BpiI and ligase into vector pAGM8031 thus resulting in level M construct pAGB1200.

For the generation of level P constructs, level M constructs pAGB763 (T3S gene cluster with deletions in *hrcQ* and *hrcJ*), pAGB794 (T3S gene cluster with a deletion in *hrcQ* and a frameshift mutation in *hrpB4*), pAGB871 (T3S gene cluster with deletions in *hrcQ* and *hrcD*) and pAGB1200 (T3S gene cluster with deletions in *hrcQ* and *hrcD* and a frameshift mutation in *hrpB4*) were individually assembled with the level M construct pAGB322 (contains *xopA*, *hpaH*, *hrpX*, *hrpG** and *hrcQ-sfgfp*) and the end-linker pICH79264 in the level P vector pICH75322 using BsaI and ligase, thus resulting in the final level P constructs pAGB766 (deletions in *hrcQ* and *hrcJ*), pAGB800 (deletion in *hrcQ* and frameshift mutation in *hrpB4*), pAGB866 (deletions in *hrcQ* and *hrcD*) and pAGB1204 (deletions in *hrcQ* and *hrcD* and frameshift mutation in *hrpB4*). All constructs are listed in Table S1 and level P constructs are summarised in Figure S8.

4.6 | Generation of modular T3S gene cluster constructs for complementation studies

For complementation studies, *hrcD*, *hrcJ* and *hrpB4* were amplified by PCR using primer pair hrcD-C-MoClo-F/hrcD-C-MoClo-R, hrcJ-C-MoClo-F/hrcJ-C-MoClo-R and hrpB4-C-MoClo-F/hrpB4-C-MoClo-R, respectively. Amplified *hrcD* and *hrcJ* genes were individually cloned into vector pICH41021 using SmaI and ligase. The *hrpB4* amplicon was cloned into vector pAGM9121 using BpiI and ligase. The inserts of the resulting level-2 constructs pAGB604 (*hrcJ*), pAGB610 (*hrcD*) and pAGB936 (*hrpB4*) were individually cloned into the level-1 pAGM1311 vector, using BsaI and ligase, thus generating constructs pAGB475, pAGB476 and pAGB938. For the generation of *sfgfp* fusions, *sfgfp* was amplified from construct pAGB322 using primers N-sfGFP-MoClo-F/N-sfGFP-MoClo-R and cloned as blunt-end fragment using SmaI and ligase into vector pICH41021, thus leading to construct pAGB488. The primers introduced a linker (AKLEGPAGL)-encoding sequence between *sfgfp* and the fusion partners. Level-1 modules corresponding to *hrcJ* (pAGB475), *hrcD* (pAGB476) and *hrpB4* (pAGB938) were assembled with *sfgfp* (pAGB488) in vector pICH41308 to generate the level 0 constructs pAGB829 (*sfgfp-hrcD*), pAGB830 (*sfgfp-hrcJ*) and pAGB942 (*sfgfp-hrpB4*).

To express the reporter gene fusions under control of the native promoters, the *hrpB* operon promoter (*phrpB*) was amplified from construct pAGB197 using primers PhrpB-F-MoClo/PhrpB-R-MoClo and the *hrpE* operon promoter (*phrpE*) from construct pAGB206 using primers PhrpE-F-MoClo/PhrpE-R-MoClo. The amplicons were cloned blunt end using SmaI and ligase into vector pICH41021, resulting in level-1 constructs pAGB615 (*phrpB*) and pAGB616 (*phrpE*), and subsequently transferred into vector pICH41295 using BpiI and ligase to generate level 0 constructs pAGB512 (*phrpB*) and pAGB513 (*phrpE*). Promoter fragments and *sfgfp* fusions were assembled in level 1 vector pICH47781 using BsaI and ligase, resulting in constructs pAGB835 (*phrpE-sfgfp-hrcD*), pAGB837 (*phrpB-sfgfp-hrcJ*) and pAGB946 (*phrpB-sfgfp-hrpB4*). All constructs included a transcriptional terminator from *X. campestris pv. vesicatoria* (construct pAGB231). The *sfgfp* fusion modules were individually assembled with inserts from constructs pAGB157 (containing *hpaH*), pICH54066 (dummy pos. 6), pAGB160 (containing *hrpX*), pAGB163 (containing *hrpG**), pICH54022 (dummy pos. 2′) and pICH50881 (Level M end-linker) in vector pAGM8079 using BpiI and ligase, thus generating level M constructs pAGB843 (including *sfgfp-hrcD*), pAGB845 (including *sfgfp-hrcJ*) and pAGB950 (including *sfgfp-hrpB4*).

Level M constructs containing *sfgfp-hrcD*, *sfgfp-hrcJ* or *sfgfp-hrpB4* were assembled in the level P vector with additional level M constructs containing mutations in *hrpB4*, *hrcJ* or *hrcD*. To generate a level M construct containing the *hrp* gene cluster with a deletion in *hrcD*, the inserts of constructs pAGB210 (contains the *hrpC* operon, *phrpE*, *hrcQ* and *hrcR*) and pAGB261 (contains *hrcS*, *hpaA*, a deletion in *hrcD*, *hrpD6*, *hrpE*, *hpaB* and *hpaE*) were assembled in vector pICH41331 using BpiI and ligase, thus generating construct pAGB732. The corresponding insert was subsequently transferred into vector pICH47751 using BsaI and ligase and leading to the level 1 construct pAGB735. The inserts of constructs pAGB735, pAGB154 (contains the *hrpA* and *hrpB* operon) and pAGB156 (contains *hrpF*), as well as the dummy module pICH54011 and the end-linker pICH50900 were assembled in vector pAGM8031 using BpiI and ligase, resulting in construct pAGB740 (contains the *hrp* cluster with a deletion in *hrcD*). For the introduction of a frameshift mutation into *hrpB4* in the T3S gene cluster, the inserts of constructs pAGB788 (contains the *hrpA* and *hrpB* operon with a frameshift mutation in *hrpB4*), pAGB155 (contains the *hrpC*, *hrpD*, *hrpE* and *hpaB* operons), pAGB156 (contains *hrpF*), the dummy module pICH54011 and the end-linker pICH50900 were assembled in vector pAGM8031, thus generating the level M construct pAGB932. To generate a level M construct with a deletion in *hrcJ*, the inserts of construct pAGB682 (contains the *hrpA* and *hrpB* operon with a deletion in *hrcJ*), pAGB155, pAGB156, the dummy module pICH54011 and the end-linker pICH50900 were assembled in vector pAGM8031, thus generating the level M construct pAGB738.

Level M modules containing the T3S gene cluster with mutations in *hrpB4*, *hrcD* and *hrcJ*, respectively, were assembled with level M modules containing the regulatory and accessory genes and the corresponding *sfgfp* fusion in vector pICH75322 using the end-linker pICH79264, BsaI and ligase. The corresponding level P constructs are pAGB851 (*hrp-HAGX* construct with a deletion in *hrcD* and containing *sfgfp-hrcD*), pAGB853 (*hrp-HAGX* construct with a deletion in *hrcJ* and containing *sfgfp-hrcJ*) and pAGB954 (*hrp-HAGX* construct with a frameshift mutation in *hrpB4* and containing *sfgfp-hrpB4*). All level P constructs are shown in Figure S8.

4.7 | Analysis of in vitro T3S

In vitro T3S assays were performed as described previously (Rossier, Wengelnik, Hahn, & Bonas, 1999). Briefly, bacteria were grown overnight in MA medium pH 7.0 supplemented with sucrose (10 mM) and casamino acids (0.3%) and shifted to MA medium pH 5.3 containing 50 μg/mL BSA (bovine serum albumin) and 10 μM thiamine at an optical density at 600 nm (OD_{600}) of 0.15. Cultures were incubated on a rotary shaker for 1.5 h at 30°C, and bacterial cells and secreted proteins were separated by filtration. Proteins in 2 mL of the culture supernatants were precipitated with trichloroacetic acid and resuspended in 20 μL Laemmli buffer. Experiments were performed three times with similar results.

4.8 | Immunodetection of proteins

Protein extracts were analysed by SDS-PAGE and immunoblotting, using antibodies directed against the c-Myc and FLAG epitope, GST, HrpF, HrcJ, HrcN and HrpB1, respectively (Büttner, Nennstiel, Klüsener, & Bonas, 2002; Rossier et al., 2000). Horseradish peroxidase-labelled anti-mouse, anti-rabbit and anti-goat antibodies were used as secondary antibodies. Binding of antibodies was visualised by enhanced chemiluminescence.

4.9 | GST pull-down assays

For GST pull-down assays, *E. coli* BL21(DE3) cells containing the expression constructs for the synthesis of GST, GST-HrpB4 and C-terminally c-Myc epitope-tagged potential interaction partners were grown in LB medium until an OD_{600} of 0.6–0.8. Gene expression, which was driven in all cases by the *lac* promoter, was induced in the presence of IPTG (isopropyl-β-D-thiogalactopyranoside; 2 mM final concentration) for 2 h at 37°C and after centrifugation bacterial cells were broken with a French press. Cell debris were removed by centrifugation, and soluble GST and GST fusion proteins were immobilised on a glutathione sepharose matrix according to the manufacturer's instructions (GE Healthcare). After washing of the matrix, immobilised GST and GST-HrpB4 were incubated with bacterial lysates containing the predicted interaction partner for 2 h at 4°C on an overhead shaker. Unbound proteins were removed by washing and bound proteins were eluted with Laemmli buffer. Cell lysates and eluted proteins were analysed by SDS-PAGE and immunoblotting. Experiments were performed three times with similar results.

4.10 | Fractionation experiments with *Xcv* strains

To analyse the subcellular localization of HrpB4, bacteria were grown overnight in MA medium (pH 7.0) as described above. Bacteria from overnight cultures were used to inoculate 50 mL MA (pH 5.3) containing BSA and thiamine as described above with an OD_{600} of 0.1 in MA pH 7.0 and an OD_{600} of 0.2 in MA pH 5.3. We used an OD_{600} of 0.2 in MA pH 5.3 due to the slower bacterial growth at pH 5.3. The cultures were grown overnight at 30°C on a shaker. Cells were then harvested by centrifugation, resuspended in 2 mL 200 mM HEPES (4-[2-hydroxyethyl]-1-piperazinylethanesulfonic acid) and lysed with a French press. After removing the cell debris via centrifugation, the lysates were centrifuged at 200.000×*g* for 90 min at 4°C. A sample from the supernatant representing the soluble fraction was taken. The pellet corresponding to the membrane fraction was stirred in 1 mL 200 mM HEPES supplemented with 5 M urea for 1 h at 4°C. The solution was centrifuged as above and a sample corresponding to the membrane-associated fraction was taken from the supernatant. The pellet, corresponding the integral membrane protein fraction, was resuspended in 200 mM HEPES. All samples were mixed with Laemmli and analysed by SDS-PAGE and immunoblotting. Experiments were performed three times with similar results.

4.11 | Fluorescence microscopy analyses

HrcQ-sfGFP foci formation was analysed in bacteria grown overnight in MA pH 7.0 and resuspended to an OD_{600} of 0.15 in MA pH 5.3 supplemented with BSA (50 μg/mL) and thiamine (10 μg/mL) as described above. The bacteria were incubated on a tube rotator at 30°C for 1 h and placed on a microscopy slide on top of a pad of 1% agarose dissolved in MA pH 5.3 with BSA and thiamine as described previously (Hausner et al., 2019). GFP fluorescence was inspected with a confocal laser scanning microscope (Zeiss LSM 780 AxioObserver. Z1) using filter sets for sfGFP (excitation at 485 nm; emission at 510 nm). Experiments were performed with different transconjugants for each strain at least three times with similar results. Fluorescent foci were counted in approximately 300 cells of three transconjugants for each strain. Results from one representative experiment are shown.

4.12 | BACTH assays

BACTH assays were performed on the basis of the Euromedex BACTH system kit. We modified the vectors for cloning purposes as described above. Expression constructs were transformed into JM109 *E. coli* cells to test protein synthesis. For this, bacterial cultures were induced with IPTG at an OD_{600} of 0.6–0.8 and incubated on a rotary shaker for 2 h at 37°C. Bacterial cells were collected by centrifugation, resuspended in Laemmli buffer and analysed by immunoblotting, using a FLAG epitope-specific antibody. For protein–protein interaction studies, expression constructs encoding T18- and T25-fusion proteins were cotransformed into chemically competent DHM1 or BTH101 *E. coli* strains and transformands were plated on LB plates containing kanamycin and gentamicin (Karimova et al., 2005). At least three colonies per transformand were used to inoculate LB overnight cultures with appropriate antibiotics, which were incubated at 30°C on a rotary shaker. Two microlitres of the overnight cultures were spotted on LB plates containing appropriate antibiotics, X-gal (5-bromo-4-chloro-3-indolyl-β-D-galactopyranosid; 40 μg/mL) and 2 mM IPTG.

Plates were photographed after 3 days of incubation at 30°C or at room temperature. Every co-transformation was performed at least three times; representative results are shown.

ACKNOWLEDGEMENTS

We thank T. Seifert for generating the modified BACTH vectors, S. Thieme and U. Bonas for providing the *eforRed* template, and U. Bonas for helpful comments on the manuscript. This study was supported by grants from the Deutsche Forschungsgemeinschaft (BU2145/9-1 and BU2145/10-1) to D.B. Open access funding enabled and organized by Projekt DEAL.

CONFLICT OF INTEREST

The authors declare no conflict of interest.

DATA AVAILABILITY STATEMENT

The data that support the findings of this study are available from the corresponding author upon reasonable request.

ORCID

Daniela Büttner https://orcid.org/0000-0003-3702-4172

REFERENCES

Alfano, J. R., & Collmer, A. (1997). The type III (Hrp) secretion pathway of plant pathogenic bacteria: Trafficking harpins, Avr proteins, and death. *Journal of Bacteriology*, *179*, 5655–5662.

Ausubel, F. M., Brent, R., Kingston, R. E., Moore, D. D., Seidman, J. G., Smith, J. A., & Struhl, K. (Eds.). (1996). *Current protocols in molecular biology*. New York, NY: Wiley.

Battesti, A., & Bouveret, E. (2012). The bacterial two-hybrid system based on adenylate cyclase reconstitution in *Escherichia coli*. *Methods*, *58*, 325–334.

Berger, C., Robin, G. P., Bonas, U., & Koebnik, R. (2010). Membrane topology of conserved components of the type III secretion system from the plant pathogen *Xanthomonas campestris* pv. *vesicatoria*. *Microbiology*, *156*, 1963–1974.

Bogdanove, A., Beer, S. V., Bonas, U., Boucher, C. A., Collmer, A., Coplin, D. L., et al. (1996). Unified nomenclature for broadly conserved *hrp* genes of phytopathogenic bacteria. *Molecular Microbiology*, *20*, 681–683.

Büttner, D. (2012). Protein export according to schedule—Architecture, assembly and regulation of type III secretion systems from plant and animal pathogenic bacteria. *Microbiology and Molecular Biology Reviews*, *76*, 262–310.

Büttner, D. (2016). Behind the lines—Actions of bacterial type III effector proteins in plant cells. *FEMS Microbiology Reviews*, *40*, 894–937.

Büttner, D., & Bonas, U. (2002). Getting across - bacterial type III effector proteins on their way to the plant cell. *EMBO Journal*, *21*, 5313–5322.

Büttner, D., & Bonas, U. (2010). Regulation and secretion of *Xanthomonas* virulence factors. *FEMS Microbiology Reviews*, *34*, 107–133.

Büttner, D., Nennstiel, D., Klüsener, B., & Bonas, U. (2002). Functional analysis of HrpF, a putative type III translocon protein from *Xanthomonas campestris* pv. *vesicatoria*. *Journal of Bacteriology*, *184*, 2389–2398.

Daniels, M. J., Barber, C. E., Turner, P. C., Cleary, W. G., & Sawczyc, M. K. (1984). Isolation of mutants of *Xanthomonas campestris* pathovar *campestris* showing altered pathogenicity. *Journal of General Microbiology*, *130*, 2447–2455.

Deng, W., Marshall, N. C., Rowland, J. L., McCoy, J. M., Worrall, L. J., Santos, A. S., … Finlay, B. B. (2017). Assembly, structure, function and regulation of type III secretion systems. *Nature Reviews Microbiology*, *15*, 323–337.

Diepold, A., Amstutz, M., Abel, S., Sorg, I., Jenal, U., & Cornelis, G. R. (2010). Deciphering the assembly of the *Yersinia* type III secretion injectisome. *EMBO Journal*, *29*, 1928–1940.

Diepold, A., Kudryashev, M., Delalez, N. J., Berry, R. M., & Armitage, J. P. (2015). Composition, formation, and regulation of the cytosolic c-ring, a dynamic component of the type III secretion injectisome. *PLoS Biology*, *13*, e1002039.

Diepold, A., Sezgin, E., Huseyin, M., Mortimer, T., Eggeling, C., & Armitage, J. P. (2017). A dynamic and adaptive network of cytosolic interactions governs protein export by the T3SS injectisome. *Nature Communications*, *8*, 15940.

Drehkopf, S., Otten, C., Hausner, J., Seifert, T., & Büttner, D. (2020). HrpB7 from *Xanthomonas campestris* pv. *vesicatoria* is an essential component of the type III secretion system and shares features of HrpO/FliJ/YscO family members. *Cellular Microbiology*, *22*, e13160.

Engler, C., Kandzia, R., & Marillonnet, S. (2008). A one pot, one step, precision cloning method with high throughput capability. *PLoS One*, *3*, e3647.

Ghosh, P. (2004). Process of protein transport by the type III secretion system. *Microbiology and Molecular Biology Reviews*, *68*, 771–795.

Gill, U. S., Lee, S., & Mysore, K. S. (2015). Host versus nonhost resistance: Distinct wars with similar arsenals. *Phytopathology*, *105*, 580–587.

Hausner, J., Hartmann, N., Jordan, M., & Büttner, D. (2017). The predicted lytic transglycosylase HpaH from *Xanthomonas campestris* pv. *vesicatoria* associates with the type III secretion system and promotes effector protein translocation. *Infection and Immunity*, *85*, e00788–e00716.

Hausner, J., Jordan, M., Otten, C., Marillonnet, S., & Büttner, D. (2019). Modular cloning of the type III secretion gene cluster from the plant-pathogenic bacterium *Xanthomonas euvesicatoria*. *ACS Synthetic Biology*, *8*, 532–547.

Hu, B., Lara-Tejero, M., Kong, Q., Galan, J. E., & Liu, J. (2017). In situ molecular architecture of the *Salmonella* type III secretion machine. *Cell*, *168* (1065–1074), e1010.

Hu, B., Morado, D. R., Margolin, W., Rohde, J. R., Arizmendi, O., Picking, W. L., … Liu, J. (2015). Visualization of the type III secretion sorting platform of *Shigella flexneri*. *Proceedings of the National Academy of Sciences USA*, *112*, 1047–1052.

Jones, J. B., Lacy, G. H., Bouzar, H., Stall, R. E., & Schaad, N. W. (2004). Reclassification of the xanthomonads associated with bacterial spot disease of tomato and pepper. *Systematic and Applied Microbiology*, *27*, 755–762.

Jones, J. D., & Dangl, J. L. (2006). The plant immune system. *Nature*, *444*, 323–329.

Karimova, G., Dautin, N., & Ladant, D. (2005). Interaction network among *Escherichia coli* membrane proteins involved in cell division as revealed by bacterial two-hybrid analysis. *Journal of Bacteriology*, *187*, 2233–2243.

Karimova, G., Pidoux, J., Ullmann, A., & Ladant, D. (1998). A bacterial two-hybrid system based on a reconstituted signal transduction pathway. *Proceedings of the National Academy of Sciences USA*, *95*, 5752–5756.

Karimova, G., Ullmann, A., & Ladant, D. (2001). Protein-protein interaction between *Bacillus stearothermophilus* tyrosyl-tRNA synthetase subdomains revealed by a bacterial two-hybrid system. *Journal of Molecular Microbiology and Biotechnology*, *3*, 73–82.

Kawamoto, A., Morimoto, Y. V., Miyata, T., Minamino, T., Hughes, K. T., Kato, T., & Namba, K. (2013). Common and distinct structural features of *Salmonella* injectisome and flagellar basal body. *Scientific Reports*, *3*, 3369.

Kousik, C. S., & Ritchie, D. F. (1998). Response of bell pepper cultivars to bacterial spot pathogen races that individually overcome major resistance genes. *Plant Disease*, *82*, 181–186.

Lara-Tejero, M. (2019). The type III secretion system sorting platform. *Current Topics of Microbial Immunology*, *427*, 133–142.

Lara-Tejero, M., & Galan, J. E. (2019). The injectisome, a complex nanomachine for protein injection into mammalian cells. *EcoSal Plus*, *8*. https://doi.org/10.1128/ecosalplus.ESP-0039-2018.

Liljeruhm, J., Funk, S. K., Tietscher, S., Edlund, A. D., Jamal, S., Wistrand-Yuen, P., et al. (2018). Engineering a palette of eukaryotic chromoproteins for bacterial synthetic biology. *Journal of Biological Engineering*, *12*, 8.

Lorenz, C., & Büttner, D. (2009). Functional characterization of the type III secretion ATPase HrcN from the plant pathogen Xanthomonas campestris pv. vesicatoria. *Journal of Bacteriology*, *191*, 1414–1428.

Lorenz, C., Hausner, J., & Büttner, D. (2012). HrcQ provides a docking site for early and late type III secretion substrates from *Xanthomonas*. *PLoS One*, *7*, e51063.

Minsavage, G. V., Dahlbeck, D., Whalen, M. C., Kearny, B., Bonas, U., Staskawicz, B. J., & Stall, R. E. (1990). Gene-for-gene relationships specifying disease resistance in *Xanthomonas campestris* pv. *vesicatoria*—Pepper interactions. *Molecular Plant-Microbe Interactions*, *3*, 41–47.

Muthuramalingam, M., Whittier, S. K., Lovell, S., Battaile, K. P., Tachiyama, S., Johnson, D. K., … Picking, W. D. (2020). The structures of SctK and SctD from *Pseudomonas aeruginosa* reveal the interface of the type III secretion system basal body and sorting platform. *Journal of Molecular Biology*, *432*, 166693.

Noël, L., Thieme, F., Nennstiel, D., & Bonas, U. (2002). Two novel type III system-secreted proteins of *Xanthomonas campestris* pv. vesicatoria are encoded within the *hrp* pathogenicity island. *Journal of Bacteriology*, *184*, 1340–1348.

Notti, R. Q., Bhattacharya, S., Lilic, M., & Stebbins, C. E. (2015). A common assembly module in injectisome and flagellar type III secretion sorting platforms. *Nature Communications*, *6*, 7125.

Rocha, J. M., Richardson, C. J., Zhang, M., Darch, C. M., Cai, E., Diepold, A., & Gahlmann, A. (2018). Single-molecule tracking in live *Yersinia enterocolitica* reveals distinct cytosolic complexes of injectisome subunits. *Integrative Biology*, *10*, 502–515.

Rossier, O., Van den Ackerveken, G., & Bonas, U. (2000). HrpB2 and HrpF from *Xanthomonas* are type III-secreted proteins and essential for pathogenicity and recognition by the host plant. *Molecular Microbiology*, *38*, 828–838.

Rossier, O., Wengelnik, K., Hahn, K., & Bonas, U. (1999). The *Xanthomonas* Hrp type III system secretes proteins from plant and mammalian pathogens. *Proceedings of the National Academy of Sciences USA*, *96*, 9368–9373.

Singh, N., & Wagner, S. (2019). Investigating the assembly of the bacterial type III secretion system injectisome by *in vivo* photocrosslinking. *International Journal of Medical Microbiology*, *309*, 151331.

Soto, E., Espinosa, N., Diaz-Guerrero, M., Gaytan, M. O., Puente, J. L., & Gonzalez-Pedrajo, B. (2017). Functional characterization of EscK (Orf4), a sorting platform component of the enteropathogenic *Escherichia coli* injectisome. *Journal of Bacteriology*, *199*, e00538–e00516.

Tachiyama, S., Chang, Y., Muthuramalingam, M., Hu, B., Barta, M. L., Picking, W. L., … Picking, W. D. (2019). The cytoplasmic domain of MxiG interacts with MxiK and directs assembly of the sorting platform in the *Shigella* type III secretion system. *Journal of Biological Chemistry*, *294*, 19184–19196.

Tampakaki, A. P., Skandalis, N., Gazi, A. D., Bastaki, M. N., Sarris, P. F., Charova, S. N., … Panopoulos, N. J. (2010). Playing the "Harp": Evolution of our understanding of *hrp/hrc* genes. *Annual Review of Phytopathology*, *48*, 347–370.

Timilsina, S., Potnis, N., Newberry, E. A., Liyanapathiranage, P., Iruegas-Bocardo, F., White, F. F., … Jones, J. B. (2020). *Xanthomonas* diversity, virulence and plant-pathogen interactions. *Nature Reviews Microbiology*, *18*, 415–427.

Troisfontaines, P., & Cornelis, G. R. (2005). Type III secretion: More systems than you think. *Physiologia Plantarum*, *20*, 326–339.

Wagner, S., Grin, I., Malmsheimer, S., Singh, N., Torres-Vargas, C. E., & Westerhausen, S. (2018). Bacterial type III secretion systems: A complex device for the delivery of bacterial effector proteins into eukaryotic host cells. *FEMS Microbiology Letters*, *365*, fny201.

Wengelnik, K., & Bonas, U. (1996). HrpXv, an AraC-type regulator, activates expression of five of the six loci in the *hrp* cluster of *Xanthomonas campestris* pv. vesicatoria. *Journal of Bacteriology*, *178*, 3462–3469.

Wengelnik, K., Rossier, O., & Bonas, U. (1999). Mutations in the regulatory gene *hrpG* of *Xanthomonas campestris* pv. vesicatoria result in constitutive expression of all *hrp* genes. *Journal of Bacteriology*, *181*, 6828–6831.

Wengelnik, K., Van den Ackerveken, G., & Bonas, U. (1996). HrpG, a key *hrp* regulatory protein of *Xanthomonas campestris* pv. *vesicatoria* is homologous to two-component response regulators. *Molecular Plant-Microbe Interactions*, *9*, 704–712.

Zhang, Y., Lara-Tejero, M., Bewersdorf, J., & Galan, J. E. (2017). Visualization and characterization of individual type III protein secretion machines in live bacteria. *Proceedings of the National Academy of Sciences USA*, *114*, 6098–6103.

SUPPORTING INFORMATION

Additional supporting information may be found online in the Supporting Information section at the end of this article.

How to cite this article: Otten C, Büttner D. HrpB4 from *Xanthomonas campestris pv. vesicatoria* acts similarly to SctK proteins and promotes the docking of the predicted sorting platform to the type III secretion system. *Cellular Microbiology*. 2021;23:e13327. https://doi.org/10.1111/cmi.13327